TM-71-2014-6

TECHNICAL MEMORANDUM

LUNAR GRAVITY DERIVED FROM LONG-PERIOD SATELLITE MOTION — A PROPOSED METHOD

Bellcomm

BELLCOMM, INC.
955 L'ENFANT PLAZA NORTH, S.W. WASHINGTON, D.C. 20024

COVER SHEET FOR TECHNICAL MEMORANDUM

TITLE- Lunar Gravity Derived from Long-Period Satellite Motion - A Proposed Method

TM-71-2014-6

DATE- November 29, 1971

FILING CASE NO(S)- 310

AUTHOR(S)- A. J. Ferrari

FILING SUBJECT(S)-
(ASSIGNED BY AUTHOR(S)- Selenodesy, Perturbation Theory, Celestial Mechanics

ABSTRACT

A new method has been devised to determine the spherical harmonic coefficients of the lunar gravity field. This method consists of a two-step data reduction and estimation process. In the first step, a weighted least-squares empirical orbit determination scheme is applied to Doppler tracking data from lunar orbits to estimate long-period Kepler elements and rates. Each of the Kepler elements is represented by an independent function of time. The long-period perturbing effects of the earth, sun, and solar radiation are explicitly modeled in this scheme. Kepler element variations estimated by this empirical processor are then ascribed to the non-central lunar gravitation features. Doppler data are reduced in this manner for as many orbits as are available. In the second step, the Kepler element rates are used as input to a second least-squares processor that estimates lunar gravity coefficients using the long-period Lagrange perturbation equations.

Pseudo Doppler data have been generated simulating two different lunar orbits. This analysis included the perturbing effects of the L1 lunar gravity field, the earth, the sun, and solar radiation pressure. Orbit determinations were performed on these data and long-period orbital elements obtained. The Kepler element rates from these solutions were used to recover L1 lunar gravity coefficients. Overall results of this controlled experiment show that lunar gravity coefficients can be accurately determined and that the method is dynamically consistent with long-period perturbation theory.

SEE REVERSE SIDE FOR DISTRIBUTION LIST

DISTRIBUTION

COMPLETE MEMORANDUM TO

CORRESPONDENCE FILES:

OFFICIAL FILE COPY
plus one white copy for each additional case referenced

TECHNICAL LIBRARY (4)

NASA Headquarters

R. J. Allenby/MAL
A. S. Lyman/MR
W. T. O'Bryant/MAL
W. E. Stoney/MAE

Goddard Space Flight Center

J. Barsky/554
J. P. Murphy/552

Langley Research Center

W. H. Michael, Jr./152A
R. H. Tolson/152A

Manned Spacecraft Center

J. P. Mayer/FM4
J. C. McPherson/FM4
E. R. Schiesser/FM4
R. K. Osburn/FM4
W. R. Wollenhaupt/FM4

Jet Propulsion Laboratory

G. H. Born/CPB-212B
P. Gottlieb/156-223
J. Lorell/CPB-202
P. Mullen/CPB-104
W. L. Sjogren/CPB-212B
J. F. Jordan/CPB-212B
A. Liu/CPB-212B
W. I. McLaughlin/156-229

Aerospace Corporation

L. Wong

BA-146 (8-64)

COMPLETE MEMORANDUM TO

Mass. Institute of Technology

R. H. Battin

Bell Telephone Laboratories

W. M. Boyce/MH
F. T. Geyling/WH
A. G. Lubowe/WH
B. G. Niedfeldt/WH

University of California

W. M. Kaula

Computer Science Corp.

D. H. Novak

Bellcomm Inc.

R. A. Bass
A. P. Boysen, Jr.
J. O. Cappellari, Jr.
D. A. DeGraaf
F. El-Baz
D. R. Hagner
W. G. Heffron
N. W. Hinners
T. B. Hoekstra
M. Liwshitz
J. L. Marshall, Jr.
K. E. Martersteck
J. Z. Menard
P. E. Reynolds
R. V. Sperry
J. W. Timko
R. L. Wagner
Department 1024 File
Central Files

Abstract only to

NASA Headquarters

R. A. Petrone/MA

Bellcomm, Inc.

J. P. Downs
I. M. Ross
M. P. Wilson

Bellcomm

955 L'Enfant Plaza North, S.W.
Washington, D. C. 20024

TM71-2014-6

date: November 29, 1971

to: Distribution

from: A. J. Ferrari

subject: Lunar Gravity Derived from Long-Period Satellite Motion - A Proposed Method - Case 310

TECHNICAL MEMORANDUM

INTRODUCTION

The long-period motion of a close lunar satellite is governed by a perturbed Newtonian gravitational law of attraction. The principal perturbations arise from the non-central properties of the lunar mass distribution and from the disturbing effects of the earth, the sun, and solar radiation pressure. These perturbations are small; their effects are at least one thousand times smaller than the inverse square attraction of the moon.

For the case of satellite motion in a non-central gravity field, the long-period Kepler elements of the orbit become complex functions of time. One method of representing this motion is to model each of the Kepler elements as independent time functions[1]. This representation forms the basis of an empirical orbit determination and selenodesy method. In this approach, gravitational effects are determined, hence the concept is not constrained to any assumed lunar gravity model. Since expressions for both third body and solar radiation perturbations are well known[2,3], the long-period variations in the orbital elements can be adjusted to remove these effects. The resulting orbital element variations can therefore be ascribed to non-central lunar gravity features.

Spherical harmonic coefficients in the lunar gravity field are determined using a two-step data reduction and estimation process. In the first step, a weighted least-squares orbit determination processor is applied to Doppler tracking data from lunar orbits to estimate long-period Kepler elements and rates. In the second step, the Kepler element rates are used as input to a second weighted least-squares processor that estimates lunar gravity coefficients using the long-period Lagrange perturbation equations.

This paper presents the theory and equations which constitute this method. An example is given, using pseudo Doppler data, to show the effectiveness of the method to determine lunar gravity coefficients.

MATHEMATICAL THEORY

The dynamical state of a satellite in lunar orbit, referenced to moon-centered inertial coordinates, is uniquely specified by the six-vector of Kepler elements;

$$\bar{k} = \begin{bmatrix} a \\ e \\ I \\ \Omega \\ \omega \\ M \end{bmatrix} \tag{1}$$

The equations of motion are the six first order, non-linear, long-period Lagrange perturbation equations,

$$\frac{da}{dt} = 0 \tag{2}$$

$$\frac{de}{dt} = \frac{-1}{na^2 e}\left[\sqrt{1-e^2}\ \frac{\partial R'}{\partial \omega}\right] \tag{3}$$

$$\frac{d\omega}{dt} = \frac{\sqrt{1-e^2}}{na^2}\left[\frac{1}{e}\frac{\partial R'}{\partial e} - \frac{\cot I}{1-e^2}\frac{\partial R'}{\partial I}\right] \tag{4}$$

$$\frac{d\Omega}{dt} = \frac{\csc I}{na^2\sqrt{1-e^2}}\frac{\partial R'}{\partial I} \tag{5}$$

$$\frac{dI}{dt} = \frac{\csc I}{na^2\sqrt{1-e^2}}\left[\cos I\ \frac{\partial R'}{\partial \omega} - \frac{\partial R'}{\partial \Omega}\right] \tag{6}$$

$$\frac{dM}{dt} = n - \frac{1}{na}\left[\frac{1-e^2}{ae}\frac{\partial R'}{\partial e} + \frac{2}{\partial a}\frac{\partial R'}{}\right] \tag{7}$$

where the mean motion $n = \sqrt{\frac{\mu_{\text{(}}}{a^3}}$, $\mu_{\text{(}}$ is the lunar gravity constant and R' is the disturbing function arising from perturbations averaged over the mean anomaly.

The disturbing function assumed has components arising from the non-central part of lunar gravity, $R'_{\leftmoon}$, earth and sun perturbations, $R'_{\oplus}$ and $R'_{\odot}$, and solar radiation pressure, R_{sr}. Hence,

$$R' = R'_{\leftmoon} + R'_{\oplus} + R'_{\odot} + R'_{sr} \tag{8}$$

In vector notation the long-period perturbation equations have the following functional form:

$$\frac{d\bar{k}}{dt} = \bar{f}(\bar{k}', t) \tag{9}$$

where k' is the five vector of Kepler elements excluding the mean anomaly. In order to carry out a solution for these equations, the disturbing function must be specified.

The long-period disturbing function for non-central lunar gravity features has been derived by Kaula[4] and is given as follows:

$$R'_{\leftmoon} = \sum_{\ell=2}^{\infty} \sum_{m=o}^{\ell} \mu_{\leftmoon} \frac{R_e^{\ell}}{a^{\ell+1}} P(I,e) S_{\ell mpq}(\omega, \Omega, \theta) \tag{10}$$

where:

$$P(I,e) = \sum_{p=o}^{h} F_{\ell mp}(I) G_{\ell pq}(e) \tag{11}$$

R_e is the mean lunar radius, h is the integer part of $\frac{(\ell-m)}{2}$ and

$$F_{\ell mp}(I) = \sum_{t} \frac{(2\ell-2t)!}{t!(\ell-t)!(\ell-m-2t)!\, 2^{(2\ell-2t)}} \sin^{\ell-m-2t} I \sum_{s=o}^{m} \binom{m}{s} \cos^{s} I \sum_{c} \binom{\ell-m-2t+s}{c} \binom{m-s}{p-t-c} (-1)^{c-k} \tag{12}$$

where t is summed to the lesser of p or h, and c is summed over all values which make the binomial coefficients nonzero. The function $G_{\ell pq}(e)$ is:

$$G_{\ell pq}(e) = \frac{1}{(1-e^2)^{\ell-1/2}} \sum_{d=o}^{p'-1} \binom{\ell-1}{2d+\ell-2p'} \binom{2d+\ell-2p'}{d} \left(\frac{e}{2}\right)^{2d+\ell-2p'} \qquad (13)$$

where $q = 2p - \ell$ and

$$p' = p \quad \text{for} \quad p \leq \ell/2$$

$$p' = \ell - p \quad \text{for} \quad p \geq \ell/2$$

Finally the function $S_{\ell mpq}$ is

$$S_{\ell mpq} = \begin{bmatrix} C_{\ell m} \\ -S_{\ell m} \end{bmatrix} \begin{matrix} \ell-m \text{ even} \\ \ell-m \text{ odd} \end{matrix} \cos[(\ell-2p)\omega + m(\Omega-\theta)]$$

$$+ \begin{bmatrix} S_{\ell m} \\ -C_{\ell m} \end{bmatrix} \begin{matrix} \ell-m \text{ even} \\ \ell-m \text{ odd} \end{matrix} \sin[(\ell-2p)\omega + m(\Omega-\theta)] \qquad (14)$$

where θ is the angular displacement between the moon-fixed (selenographic) axis system and the inertial system. The parameters $\{C_{\ell m}, S_{\ell m}\}$ are the set of lunar harmonic coefficients which characterize the non-central parts of the gravity field.

The averaging with respect to the mean anomaly of the third body disturbing function has been performed by Lorell and Liu[5] and has the following form:

$$R_3' = \frac{\mu_3}{r_3} [F_2' + F_3'] \qquad (15)$$

where:

$$F_2' = \left(\frac{a}{r_3}\right)^2 \frac{1}{2}\left[-(1 + \frac{3}{2}e^2) + 3A^2(2e^2 + \frac{1}{2}) + \frac{3B^2}{2}(1-e^2)\right]$$

$$F_3' = \left(\frac{a}{r_3}\right)^3 A\, e\left[3(1 + \frac{3}{4}e^2) - 5A^2(e^2 + \frac{3}{4}) - \frac{15B^2}{4}(1-e^2)\right]$$

and $A = \bar{u}\cdot\bar{P}$, $B = \bar{u}\cdot\bar{Q}$. $\bar{u}$ is the unit vector in the direction of the third body, $\bar{P}$ is a unit vector to perifocus and $\bar{Q}$ is a unit vector in the orbit plane orthogonal to $\bar{P}$ (see Figure 1).

The disturbing function for solar radiation pressure has been calculated by Fisher[6] and is given as follows:

$$R'_{sr} = \frac{1}{2\pi}\int_0^{2\pi} R_{sr}\, dM \tag{16}$$

where $R_{sr} = F\ \bar{r}\cdot\bar{u}_\odot$

and $\bar{u}_\odot$ is a unit vector in the direction of the sun and F is the magnitude of solar acceleration:

$$F = \frac{\tilde{A}}{m}\ \frac{S_\odot}{c_\ell}\left(\frac{r_\odot}{r}\right)^2 (1+\alpha) \quad . \tag{17}$$

Here $\tilde{A}$ is the satellite effective cross-sectional area, m is the mass, $S_\odot$ is the solar constant, $r_\odot$ the distance to the sun, α is the reflection coefficient, and c_ℓ is the speed of light. The solar radiation pressure only acts on the satellite when it is in sunlight. A test to determine the visibility of the sun is (see Figure 2):

$\lvert\gamma\rvert \leq \lvert\beta\rvert$	Solar radiation perturbations are zero
$\lvert\gamma\rvert > \lvert\beta\rvert$	Solar radiation perturbations are present.

where:

$$\lvert\beta\rvert = \left\lvert\tan^{-1}\frac{R_e}{r}\right\rvert$$

$$\lvert\gamma\rvert = \left\lvert\cos^{-1}\frac{-\bar{r}\cdot\bar{r}'}{rr'}\right\rvert$$

and

$$\bar{r}' = \bar{r}_\odot - \bar{r}$$

The general form of the perturbation equations for a lunar satellite under the influence of non-central lunar gravity, earth, sun, and solar radiation effects is as follows:

$$\left.\begin{aligned}
\frac{da}{dt} &= 0 \\
\frac{de}{dt} &= \sum_{\ell,m} \frac{de_{\ell,m}}{dt} + \frac{de_{\oplus}}{dt} + \frac{de_{\odot}}{dt} + \frac{de_{sr}}{dt} \\
\frac{dI}{dt} &= \sum_{\ell,m} \frac{dI_{\ell,m}}{dt} + \frac{dI_{\oplus}}{dt} + \frac{dI_{\odot}}{dt} + \frac{dI_{sr}}{dt} \\
\frac{d\Omega}{dt} &= \sum_{\ell,m} \frac{d\Omega_{\ell,m}}{dt} + \frac{d\Omega_{\oplus}}{dt} + \frac{d\Omega_{\odot}}{dt} + \frac{d\Omega_{sr}}{dt} \\
\frac{d\omega}{dt} &= \sum_{\ell,m} \frac{d\omega_{\ell,m}}{dt} + \frac{d\omega_{\oplus}}{dt} + \frac{d\omega_{\odot}}{dt} + \frac{d\omega_{sr}}{dt} \\
\frac{dM}{dt} &= \sum_{\ell,m} \frac{dM_{\ell,m}}{dt} + \frac{dM_{\oplus}}{dt} + \frac{dM_{\odot}}{dt} + \frac{dM_{sr}}{dt}
\end{aligned}\right\} \qquad (18)$$

where the sum over ℓ and m represents an arbitrary gravity field of degree ℓ and order m for the moon. These long-period equations form the analytical basis for the development of the empirical orbit determination method.

The long-period time dependence induced in each of the Kepler elements by the non-central gravity perturbations has been specified by equation(18). Since these equations are non-linear, general closed form solutions are not obtainable. Since the non-central effects are extremely small compared to the central body term, solutions can be approximated by a finite series.

If an analytic quadrature is performed on each perturbation equation, a set of integral equations results:

$$\bar{k}(t) = \bar{k}(t_o) + \int_{t_o}^{t} \bar{f}(\bar{k}', t)\, dt \qquad (19)$$

The kernels, or disturbing functions, appearing in this equation are non-separable, non-linear functions. If only the perturbations arising from the lunar disturbing functions are considered, these kernels can be categorized into two types:

1. $\bar{f}(\bar{k}',t) = \bar{f}(\bar{k}')$ autonomous (20)

2. $\bar{f}(\bar{k}',t) = \bar{g}(\bar{k}')\sin m\ \omega_{\leftmoon} t + \bar{h}(\bar{k}')\cos m\ \omega_{\leftmoon} t$ (21)

$m = 2,3,.....$

where $\omega_{\leftmoon}$ is the rotational rate of the moon about its spin axis ($\omega_{\leftmoon} = .26617033 \times 10^{-6}$ rad/sec) and m is the order index for the spherical harmonic terms of the lunar gravity field. This categorization does not apply when the standard Kepler elements become singular, for nearly circular, nearly equatorial orbits. However, a similar approximation can be made for a determinate orbital element set. The first or autonomous kernel corresponds to zonal perturbations and the second to tesseral and sectorial perturbations. If solutions to equation(19) are sought which are valid over periods of time of about 24 hours, and if it is assumed that the magnitude of variation in $\bar{k}'$ over these periods is small, then $\bar{f}(\bar{k}')$, $\bar{g}(\bar{k}')$, and $\bar{h}(\bar{k}')$ can be considered constant.

Solutions to equations possessing autonomous kernels (zonal perturbations) have the following simple form:

$$\bar{k}(t) = \bar{k}(t_o) + \bar{f}[\bar{k}'(t_o)](t-t_o) \tag{22}$$

These solutions have the linear properties of secular variations. Solutions for the non-autonomous kernels can be given as follows:

$$\bar{k}(t) = \bar{C}_1[\bar{k}'(t_o)] + \bar{C}_2[\bar{k}'(t_o)]\sin m\ \omega_{\leftmoon}(t-t_o) + \bar{C}_3[\bar{k}'(t_o)]\cos m\ \omega_{\leftmoon}(t-t_o) \tag{23}$$

where $\bar{C}_1$, $\bar{C}_2$, and $\bar{C}_3$ are vector constants and $\bar{C}_1(\bar{k}'(t_o)] = \bar{k}(t_o) - \bar{C}_3[\bar{k}'(t_o)]$.

Since the moon rotates with a period of 27.32 days about its spin axis, the solutions given by equation (23) for long-periodic variations arising from tesseral and sectorial terms can be further simplified. If the time period over which equation (23) is valid (approximately 24 hours) is much smaller than the period of a spherical harmonic perturbing term, this solution can be expanded in a truncated Taylor series:

$$\bar{k}(t) = \bar{C}_1[\bar{k}'(t_o)] + \bar{C}_2[\bar{k}'(t_o)][m\omega_{\mathbb{C}}(t-t_o) + \ldots\ldots] + \bar{C}_3[\bar{k}'(t_o)][1 - \frac{m^2\omega_{\mathbb{C}}^2}{2}(t-t_o)^2 + \ldots..]$$

or

$$\bar{k}(t) = \bar{\Delta}_o + \bar{\Delta}_1 t + \bar{\Delta}_2 t^2 + \ldots\ldots \tag{24}$$

where $\bar{\Delta}_j$ represent vector constants.

Hence the solutions, or functional form, for the Kepler elements which best represent secular and long-period effects are those given by equations (22) and (24). Two typical Kepler elements, $\Omega(t)$ and $e(t)$, can be represented as follows:

$$\Omega(t) = \Omega_o + \Omega_1 t \qquad \text{(secular variation)}$$

$$e(t) = e_o + e_1 t + e_2 t^2 \qquad \text{(long-period variations)}$$

The terms Ω_o, Ω_1, e_o, e_1, e_2 are Keplerian constants determined by fitting tracking data.

The six-dimensional time series used to represent the Keplerian motion of a lunar satellite is:

$$\left.\begin{aligned} a(t) &= a \quad \text{(constant)} \\ e(t) &= e_o + e_1 t + e_2 t^2 + \delta e_{\oplus} + \delta e_{\odot} + \delta e_{sr} \\ I(t) &= I_o + I_1 t + I_2 t^2 + \delta I_{\oplus} + \delta I_{\odot} + \delta I_{sr} \\ \Omega(t) &= \Omega_o + \Omega_1 t + \Omega_2 t^2 + \delta \Omega_{\oplus} + \delta \Omega_{\odot} + \delta \Omega_{sr} \\ \omega(t) &= \omega_o + \omega_1 t + \omega_2 t^2 + \delta \omega_{\oplus} + \delta \omega_o + \delta \omega_{sr} \\ M(t) &= M_o + M_1 t + M_2 t^2 \end{aligned}\right\} \tag{25}$$

The orbital element variations $\delta\bar{k}'$ are found by numerical integrations. The third body and solar radiation pressure perturbations used are those presented earlier. No explicit third body and radiation pressure perturbations are modeled for the mean anomaly. Hence the time series includes the perturbations of the moon, earth, sun, and solar radiation. The reasons for this representation are associated with the semi-major axis determination and are discussed later in this paper.

Quadratic terms are used in the time series since for time periods of about 24 hours these will adequately represent long-period perturbations of up to order seven (m = 7).

DOPPLER DATA REDUCTION

The Doppler observation ($\dot{\rho}$) is a scalar quantity that is a non-linear function of the satellite state, $\bar{k}$, the relative earth-moon configuration, and the earth-based tracking station position and rotational velocity. During the orbit determination only the estimates of the satellite state are refined. The tracking data $\dot{\rho}_{obs}$ are related to the satellite state as follows[7]

$$\dot{\rho}_{obs}(t) = \dot{\rho}[\bar{k}(t)] + \eta \tag{26}$$

where η is the random noise associated with the physical measurements. The measurement errors are assumed to have the following properties:

$$E[\eta] = 0$$
$$E[\eta^2] = \sigma^2 \tag{27}$$

where E is the expectation operator and σ^2 is the variance of the Doppler noise.

Since the Doppler is a non-linear function of the Kepler state, equation(26) must be linearized about a reference state, $\bar{k}^*(t)$. Hence:

$$\Delta\dot{\rho}(t_k) = \left(\frac{\partial\dot{\rho}}{\partial\bar{k}}\right)\Bigg|_{\bar{k}=\bar{k}^*} \Delta\bar{k}(t_k) + \eta \tag{28}$$

where:

$$\Delta\dot{\rho}(t_k) = \dot{\rho}_{obs}(t_k) - \hat{\dot{\rho}}(t_k)$$

Using a similar procedure, a linear relationship is obtained relating the Kepler state $\bar{k}$ and the Keplerian parameter vector $\bar{K}$ (n×1).

$$\bar{K} = \begin{bmatrix} a \\ e_o \\ e_1 \\ e_2 \\ I_o \\ \cdot \\ \cdot \\ M_2 \end{bmatrix} \tag{29}$$

Since the Keplerian parameters are constant over the trajectory, an expansion of $\bar{K}$ can be performed about a reference set $\bar{K}^*$ at some time t_o.

$$\Delta\bar{k} = \left(\frac{\partial\bar{k}}{\partial\bar{K}}\right)\Bigg|_{\bar{K} = \bar{K}^*} \Delta\bar{K}(t_o) \tag{30}$$

The linearized Doppler equation(28) can now be expressed in terms of the Keplerian solution parameters.

$$\Delta\dot{\rho}(t_k) = H(t_k)\Delta\bar{K}(t_o) + \eta \tag{31}$$

where:

$$H(t_k) = \left(\frac{\partial\dot{\rho}}{\partial\bar{k}}\right)\left(\frac{\partial\bar{k}}{\partial\bar{K}}\right)\Bigg|_{\bar{K} = \bar{K}^*}$$

For a batch of r Doppler measurements equation(31) can be generalized as follows:

$$\Delta\bar{\dot{\rho}} = [H]\Delta\bar{K} + \bar{\eta} + \bar{s} \tag{32}$$

where:

$\Delta\bar{\dot{\rho}}$	is the (r × 1) observation residual vector
H	is the linearized set of functions relating the observation and the Keplerian parameters (r × n)

$\Delta\bar{K}$	is the column vector of Keplerian parameter deviations (n × 1)
$\bar{\eta}$	is an (r × 1) vector of observation noise
$\bar{s}$	is an (r × 1) vector of short-periodic errors.

Since the Keplerian parameters $\bar{K}$ only represent the long-periodic dynamics of the orbit, at any point in time there will always be a systematic residual ($\bar{s}$) associated with the unmodeled short-periodic satellite variations.

The next step is to choose an estimation scheme which minimizes the observational error and yields a best estimate for the Keplerian parameters. The weighted least-squares estimator was chosen to perform the data reduction. The error function, ε, for r observations is given as follows:

$$\varepsilon = [\bar{V}^T W \bar{V}] \qquad (\bar{V} = \bar{\eta} + \bar{s})$$

or (33)

$$\varepsilon = (\Delta\bar{\rho} - H\Delta\bar{K})^T W(\Delta\bar{\rho} - H\Delta\bar{K})$$

where W is assumed to be a (r × r) diagonal matrix. For a minimum the first variation of the error function must vanish. Transposing and solving,

$$\Delta\hat{\bar{K}} = [H^T W H]^{-1} H^T W \Delta\bar{\rho} \qquad (34)$$

Since this minimization was obtained by linearizing a set of non-linear equations, the estimation is performed iteratively.

SEMI-MAJOR AXIS DETERMINATION

Studies [8] have shown that the least-squares process has convergence problems when the semi-major axis is included as an independent parameter. Since the mean motion of the orbit, even in the presence of perturbations, is nearly inversely proportional to the semi-major axis raised to the three halves power, the estimated mean motion can be used to imply a semi-major axis. The constraint equation between the mean motion and the semi-major axis must include the long-period effects of the earth, sun, solar radiation and some representation for the lunar field.

The average value of the semi-major axis (a_o) with respect to the mean anomaly is found as follows:

$$\hat{\dot{M}} = \hat{M}_1 + 2\hat{M}_2 t$$

and

$$\hat{\dot{M}} = \sqrt{\frac{\mu}{a_o^3}} + \sum_{\ell,m} \dot{M}_{\ell,m} + \dot{M}_{\oplus} + \dot{M}_{\odot} + \dot{M}_{sr} \qquad (35)$$

where $\hat{M}_1$ and $\hat{M}_2$ are the estimated Keplerian parameters. Since this is a non-linear equation in a_o, it is solved using Newton's Method.

For the case of zonal perturbations on an earth satellite, Kozai[9] has shown that a mean value of the semi-major axis $\bar{a}$ yields the average satellite position in the orbit. This value is derived such that the deviations in the position of the orbit due to perturbations averaged over the orbit yield only short-period variations.

$$\frac{1}{2\pi}\int_o^{2\pi} \delta r(\bar{a})\ dM = \sum_{\xi=1}^{\infty} b_\xi \cos(\xi M + d_\xi) \qquad (36)$$

where $\delta r = r_{osculating} - r_{long\text{-}period}$ and b_ξ and d_ξ are constants. Hence the value $\bar{a}$ yields the proper mean position over the orbit. Kozai has shown that a mean value correction in the semi-major axis is only required for even degree zonals[10] and none for tesseral and sectorial terms[11]. Analysis has shown that mean value corrections for the sun and solar radiation perturbations are on the order of one foot; hence no factor is included for these terms. A mean value correction for earth perturbations is included. The relationship between the average value a_o and the mean value $\bar{a}$ for the C_{20} and earth perturbations are presented as examples.

For C_{20}

$$\bar{a} = a_o\left[1 + \frac{3}{2} C_{20}\left(\frac{R_e}{a}\right)^2 \frac{(1-3/2\ \sin^2 I)}{(1-e^2)^{3/2}}\right]$$

For the earth

$$\bar{a} = a_o\left[1 + \left(\frac{n_\oplus}{n}\right)^2 (1-3/2 \sin^2 I)\right]$$

The general procedure for implying a mean value semi-major axis has two steps. First, the average value a_o is determined once per iteration using equation(35). Then, the mean value $\bar{a}$ is calculated as follows:

$$\bar{a} = a_o\left[1 + \sum_{\ell} \varepsilon_{\ell,o} + \varepsilon_\oplus\right]$$

for only even values of ℓ. The ε terms are the mean value corrections.

The quantity $\bar{a}$ is introduced to make long-period perturbation theory represent the average satellite orbit. Since this variable is introduced to insure compatibility between the long-period and associated rectangular equations of motion, it is only used for Doppler data reduction.

After convergence is reached, the mean anomaly rate $\dot{M}$ is adjusted to remove the earth, sun, and solar radiation effects and evaluated at the mid-point of the data span.

$$\dot{M}_{\text{(}} = \hat{M}_1 + 2\hat{M}_2 t - \dot{M}_\oplus - \dot{M}_\odot - \dot{M}_{sr} \qquad (37)$$

Here $\dot{M}_{\text{(}}$ is the mean anomaly rate arising only from lunar gravity. The average semi-major axis value, $a_{\text{(}}$, for the lunar gravity is found by solving:

$$\dot{M}_{\text{(}} = \sqrt{\frac{\mu_{\text{(}}}{a_{\text{(}}^3}} + \sum_{\ell,m} \dot{M}_{\ell,m} \qquad (38)$$

It is this value of the semi-major axis that completes the $\bar{K}$ parameter set and is used for gravity field determination. One such value of $a_{\text{(}}$ is found for each solution.

During the determination of the semi-major axis it is necessary to specify some model for the lunar gravity field in the constraint equations. Analysis has shown that the entire selenodesy process can be performed without any a priori lunar field if it is done iteratively.

SOLUTION PARAMETERS

The output from processing a batch of Doppler measurements is a best estimate for a set of Keplerian parameters, $\hat{\bar{K}}$. Since the third body and solar radiation perturbations are modeled separately in the process and the mean anomaly parameter is adjusted for these effects, the Keplerian parameters represent the variation in the Kepler elements due only to the non-central part of lunar gravity. These solution parameters give a simultaneous time history of the Kepler elements and element rates valid over the Doppler data span. A detailed block diagram of the orbit determination process is shown in Figure 3.

The time histories of the Kepler elements and rates are used as input to a second processor which fits lunar gravity harmonics to the Kepler element rates. Since the solution parameters provide continuous time functions for the orbital elements and rates they can be sampled at any desired frequency. The long-period lunar gravity effects have periods which are much greater than a typical lunar orbiter period, hence there will be no aliasing of gravity information if samples are evaluated once per satellite period. The five Kepler element rates used for gravity estimation are:

$$\dot{\bar{K}} = \begin{bmatrix} \dot{e} \\ \dot{I} \\ \dot{\Omega} \\ \dot{\omega} \\ \dot{M} \end{bmatrix}$$

Since the semi-major axis rate is zero in long-period theory, it is not used.

The five orbital element rates are simultaneously processed to obtain gravity coefficients. Since the data set consists of five different quantities ($\dot{e}$, $\dot{I}$, $\dot{\Omega}$, $\dot{\omega}$, $\dot{M}$), a weighting matrix is required to define the relative accuracy of each of the rates.

If the orbit determination processor could model the Doppler such that the residuals remaining after convergence were normally distributed random errors, the $[H^T W H]^{-1}$ matrix in equation(34) would be the covariance matrix of the $\hat{\bar{K}}$ solution. Since only long-period satellite dynamics are represented in the

process, the $[H^T WH]^{-1}$ matrix is not the covariance matrix of the process[12]. However the terms in the $[H^T WH]^{-1}$ matrix do reflect sensitivity and correlations among the solution parameters, hence it is assumed for weighting purposes that these terms can be regarded as variances and covariances in the conventional manner.

The weighting matrix for the orbital element rates, A, is a (5×5) matrix having the following form[13]:

$$A^{-1} = \begin{bmatrix} \sigma^2_{\dot{e}} & \tau_{12} & \tau_{13} & \tau_{14} & \tau_{15} \\ \tau_{21} & \sigma^2_{\dot{I}} & \cdots & & \\ \cdot & & \sigma^2_{\dot{\Omega}} & \cdots & \\ \cdot & & & \sigma^2_{\dot{\omega}} & \cdots \\ \cdot & & & & \\ \tau_{51} & \cdots & & & \sigma^2_{\dot{M}} \end{bmatrix} \qquad (39)$$

where $\sigma^2_{\dot{k}}$ are the error variances among the rates and τ_{ij} are the covariances. It is assumed that the mean error of the Keplerian parameters is zero. Each of the orbital element rates has the following form:

$$\dot{\hat{\Omega}} = \hat{\Omega}_1 + 2\hat{\Omega}_2 t$$

The variance of the error in $\dot{\hat{\Omega}}$ is found as follows:

$$\sigma^2_{\dot{\hat{\Omega}}} = E[(\hat{\Omega}_1 - \Omega_1)^2 + 4t(\hat{\Omega}_1 - \Omega_1)(\hat{\Omega}_2 - \Omega_2) + 4t^2(\hat{\Omega}_2 - \Omega_2)^2]$$

or
$$\sigma^2_{\dot{\hat{\Omega}}} = \sigma^2_{\hat{\Omega}_1} + 4t\ \mathrm{cov}(\varepsilon_{\hat{\Omega}_1}\varepsilon_{\hat{\Omega}_2}) + 4t^2\ \sigma^2_{\hat{\Omega}_2} \qquad (40)$$

where for example: $\varepsilon_{\Omega_1} = \hat{\Omega}_1 - \Omega_1$ etc.

The covariance terms among the rates (e.g. $\mathrm{cov}(\varepsilon_{\dot{\hat{\Omega}}}\varepsilon_{\dot{\hat{\omega}}})$) are formulated in a similar way:

$$\mathrm{cov}(\varepsilon_{\dot{\hat{\Omega}}}\ \varepsilon_{\dot{\hat{\omega}}}) = \mathrm{cov}(\varepsilon_{\hat{\Omega}_1}\varepsilon_{\hat{\omega}_1}) + 2t[\mathrm{cov}(\varepsilon_{\hat{\Omega}_1}\varepsilon_{\hat{\omega}_2}) + \mathrm{cov}(\varepsilon_{\hat{\Omega}_2}\varepsilon_{\hat{\omega}_1})] + 4t^2\ \mathrm{cov}(\varepsilon_{\hat{\Omega}_2}\varepsilon_{\hat{\omega}_2}) \tag{42}$$

Hence each of the entries in the A matrix can be found from the appropriate slot in the $[H^T W H]^{-1}$ matrix. The weighting matrix is automatically obtained for each set of orbital element rates.

HARMONIC COEFFICIENT ESTIMATION

The lunar gravity field determination is performed in a second weighted least-squares processor which uses as input the Kepler element rates, the estimated Kepler elements, and a weighting matrix and outputs a set of spherical harmonic coefficients (see Figure 4). The long-period perturbation equations are of the form:

$$\dot{\bar{k}} = \bar{f}(\bar{k}', \bar{p}, t) \tag{43}$$

where $\bar{p}$ is the vector (n×1) of lunar gravity coefficients:

$$\bar{p} = \begin{bmatrix} C \\ \hline S \end{bmatrix} \tag{44}$$

Since the gravity parameters appear as linear functions in the perturbation equations, equation (43) can be expressed as

$$\dot{\bar{k}} = F(\bar{k}')\ \bar{p} \tag{45}$$

where F is a (5×n) matrix of partial derivatives of the element rates with respect to the gravity coefficients:

$$F(\bar{k}') = \begin{bmatrix} \frac{\partial \dot{e}}{\partial C_{20}} \cdots \frac{\partial \dot{e}}{\partial C_{\ell m}}, \frac{\partial \dot{e}}{\partial S_{21}} \cdots \frac{\partial \dot{e}}{\partial S_{\ell m}} \\ \vdots \qquad\qquad\qquad\qquad \vdots \\ \frac{\partial \dot{M}}{\partial C_{20}} \cdots \frac{\partial \dot{M}}{\partial C_{\ell m}}, \frac{\partial \dot{M}}{\partial S_{21}} \cdots \frac{\partial \dot{M}}{\partial S_{\ell m}} \end{bmatrix} \tag{46}$$

The least-squares algorithm for the gravity coefficient estimation is as follows:

$$\underset{(n \times 1)}{\hat{\bar{p}}} = \underbrace{[F^T A F]^{-1}}_{(n \times n)} \underbrace{F^T A \dot{\bar{k}}}_{(n \times 1)} \qquad (47)$$

where $\hat{\bar{p}}$ is the best estimate of the lunar gravity parameters.

PSEUDO DATA SIMULATIONS

In order to demonstrate the method, pseudo Doppler data were generated using numerically integrated source trajectories and converged solutions obtained. The estimated Keplerian parameters from two such typical convergences are presented. In both cases the L1 Lunar gravity field[14] was assumed (see below) and the earth, sun, and solar radiation perturbations were also included. No noise or biases were added to the pseudo data.

L1 Lunar Gravity Field

$$C_{20} = -2.071 \times 10^{-4}$$
$$C_{22} = .207 \times 10^{-4}$$
$$C_{30} = .21 \times 10^{-4}$$
$$C_{31} = .34 \times 10^{-4}$$
$$C_{33} = .26 \times 10^{-5}$$

The first simulation was generated for a Lunar Orbiter V orbit (polar). The Doppler data span contains tracking from three stations (Goldstone, California, Madrid, Spain, and Woomera, Australia) and is approximately 21 hours 30 minutes in duration. The epoch data and initial conditions for this orbit are:

Epoch Date: Aug. 9, 1967 7 hours 20 min.

Initial Conditions: (Selenographic)

a = 8,324,332 ft.	e = .27618984
I = 84°.764923	Ω = 70°.2050009
ω = 1°.8616071	M = 244°.73644

The Doppler residuals ($\Delta\dot{\rho}$) associated with this convergence are shown in Figure 5. These residuals are systematic and have the general form of the unmodeled short-period orbital variations. The residuals possess a mean of .022 feet per second (fps) and a standard deviation of σ = .11 fps.

In order to determine the quality of this converged solution, comparisons are made between the numerically integrated source trajectory and the converged solution. Figures 6-8 show the variations in the six Kepler elements for both the converged solution and the source trajectory. The variations presented for the eccentricity (e) and the three Euler angles (I,Ω,ω) (see Figures 6 and 7) show the actual variations of these elements plotted on common axes. Since the variations in the mean anomaly are very large and the semi-major axis has a large magnitude, the differences in the converged solution and the source trajectory values are shown (see Figure 8). A plot of the rectangular position difference is shown in Figure 9. The 450 ft bias in position difference is relatable to the error bias in the estimated eccentricity parameter at epoch. The slight secular error in position is attributable to small errors in the mean anomaly and eccentricity rates.

The second data simulation was generated for a Lunar Orbiter III (Apollo type) orbit. This data span contains tracking data from the same three stations and is approximately 10 hours in duration. The epoch date and initial conditions for this orbit are:

Epoch Date: Aug. 30, 1967 20 hours 55 min.

Initial Conditions: (Selenographic)

a = 6,457,093 ft.	e = .04348376
I = 20°899211	Ω = 63°970000
ω = 354°05800	M = 194°90793

The Doppler residuals associated with this solution are shown in Figure 10. These residuals have a mean of -.018 fps and a standard deviation of σ = .15 fps.

Variations in the eccentricity and the Euler angles of this orbit are shown in Figures 11 and 12. Semi-major axis, mean anomaly, and position differences are shown in Figures 13 and 14. As can be seen from Figure 11 the inclination parameter has a bias error at epoch and a slight slope error. The position

difference has a bias of 400 ft. which is attributable to biases in estimates of the eccentricity and semi-major axis parameters.

The slight biases and trend errors experienced in both these solutions are a reflection of nearly equal sensitivities among some Keplerian parameters and the aliasing effects of unmodeled short-period orbit variations. The presence of these nearly equal sensitivities among the Keplerian parameters leads to high correlations in the $[H^TWH]^{-1}$ matrix. These correlations lead to linear combinations among the state parameters being estimated.

GRAVITY FIELD DETERMINATION

In order to demonstrate the capabilities of this method, the two pseudo data solutions previously presented were used to determine the L1 lunar gravity field assumed in the source trajectory. Since the orbital period of the Orbiter V satellite is 3.2 hours and the data span 21 hours, this converged solution contributes seven sets of Kepler element rates to the harmonic estimator. The Orbiter III satellite has an orbital period of 2.1 hours and a data span of 10 hours; consequently this solution contributes five sets of Kepler element rates.

The numerical values for the L1 lunar gravity field as determined from the Orbiter III and Orbiter V convergences are the following:

$$\begin{aligned} \hat{C}_{20} &= -2.090 \times 10^{-4} \\ \hat{C}_{22} &= .213 \times 10^{-4} \\ \hat{C}_{30} &= .190 \times 10^{-4} \\ \hat{C}_{31} &= .330 \times 10^{-4} \\ \hat{C}_{33} &= .270 \times 10^{-5} \end{aligned} \qquad (48)$$

Since this entire process is one of parameter identification and the A weighting matrix used is not truly the covariance matrix of the Kepler element rates, the terms on the diagonal of the $[F^TAF]^{-1}$ matrix are not the variances of the estimated terms. The normalized non-diagonal terms in the $[F^TAF]^{-1}$ matrix do yield a measure of correlation between the various pairs of terms in the solution set. The correlation matrix for this solution is:

	C_{22}	C_{30}	C_{31}	C_{33}
C_{20}	-.07	-.21	-.13	.18
C_{22}		.16	.19	-.64
C_{30}			.87	-.06
C_{31}				-.06

The relatively high correlations between both the C_{22}, C_{33} and C_{30}, C_{31} coefficient pairs reflect the inseparability of these gravity effects in the estimator. Although data from satellites of both high (I=85°) and relatively low (I=21°) inclinations were used in this solution, the presence of these correlations reflects the necessity of additional data from intermediate orbital inclinations.

In order to obtain a quantitative measure of the solution given by equation(48) a comparison is made between it and the nominal L1 values using numerically integrated equations of motion. The comparisons, covering a one day period, (starting at the same epoch and state vector) are made for both the Lunar Orbiter III and V orbits. Differences in position and velocity magnitudes and in each of the Kepler elements for each of these orbits are shown in Figures 15-22. The position deviations developed over the Lunar Orbiter V trajectory attain a maximum value of 120 ft. The velocity errors have a peak value of .08 fps. For the case of the Lunar Orbiter III trajectory the position error attains a peak value of 150 ft. and the velocity .12 fps.

SUMMARY AND CONCLUSIONS

This analysis has presented an empirical method for determining the spherical harmonic coefficients of the lunar gravity field. Long-period Kepler elements are determined using a weighted least-squares empirical orbit determination process. Each of the Kepler elements is represented by an independent time function. The long-period perturbing effects of the earth, sun, and solar radiation are modeled explicitly in this process. The lunar gravity coefficients are determined using another weighted least-squares processor which fits the Lagrange perturbation equations to the estimated Kepler rates.

Pseudo Doppler data have been generated simulating two different lunar trajectories. The perturbations included were the L1 lunar gravity field, the earth, sun, and solar

radiation pressure. Orbit determinations were performed using the empirical processor and long-period orbital element variations obtained. The Kepler element rates from these convergences were used to recover the L1 gravity field. The overall results of this controlled experiment show that lunar gravity coefficients can be determined accurately using this method and that it is dynamically consistent with long-period perturbation theory.

A. J. Ferrari

2014-AJF-hat

REFERENCES

1. Gaposchkin, E. M., "Differential Orbit Improvement," Smithsonian Institution, Special Report No. 161, 1964.

2. Cook, G. E., "Luni-Solar Perturbations of the Orbit of an Earth Satellite," The Geophysical Journal of the Royal Astronomical Society, Vol, 6, No. 3, April 1962.

3. P. Musen, "The Influence of Solar Radiation Pressure on the Motion of an Artificial Satellite," Journal of Geophysical Research, May 1960.

4. Kaula, W. M., Theory of Satellite Geodesy, Blaisdell Publishing Co., Waltham, Mass., 1966.

5. Lorell, J. and Liu, A., "Method of Averages Expansion for Artificial Satellite Application," Jet Propulsion Lab. Report 32-1513, April 1971.

6. Fisher, D., "Formulas for Long Period Radiation Pressure, Lunar and Solar Gravitational Effects on the Motion of Artificial Satellites, Goddard Space Flight Center, N6918770, Feb. 1969.

7. de Vezin, H. G., "Doppler Observing Modeling for Apollo Real-Time Orbit Determination Program," Presented at AIAA Astrodynamics Conference, Manned Spacecraft Center, Houston, Texas, Dec. 1967.

8. Izsak, I. G., "Differential Orbit Improvement with the Use of Rotated Residual," Smithsonian Institution, Special Report No. 73, 1971.

9. Kozai, Y., "The Motion of a Close Earth Satellite," Astro J., Vol. 64, 378-397, 1959.

10. Kozai, Y., "Second Order Solution of Artificial Satellite Theory Without Drag," Astro. J., Vol. 64, 446-64, 1962.

11. Kozai, Y., Smithsonian Astrophysical Observatory, Private Communication, February 1971.

12. Durbin, J., "The Fitting of Time-Series Models," Revue Inst. Int. De Stat., 233-243, 1960.

13. Battin, R. H., Astronautical Guidance, McGraw-Hill Book Co., New York, 1964.

REFERENCE-2

14. Wollenhaupt, W. R., "Apollo Orbit Determination and Navigation," Presented at AIAA 8th Aerospace Sciences Meeting, New York, N.Y., January 1970.

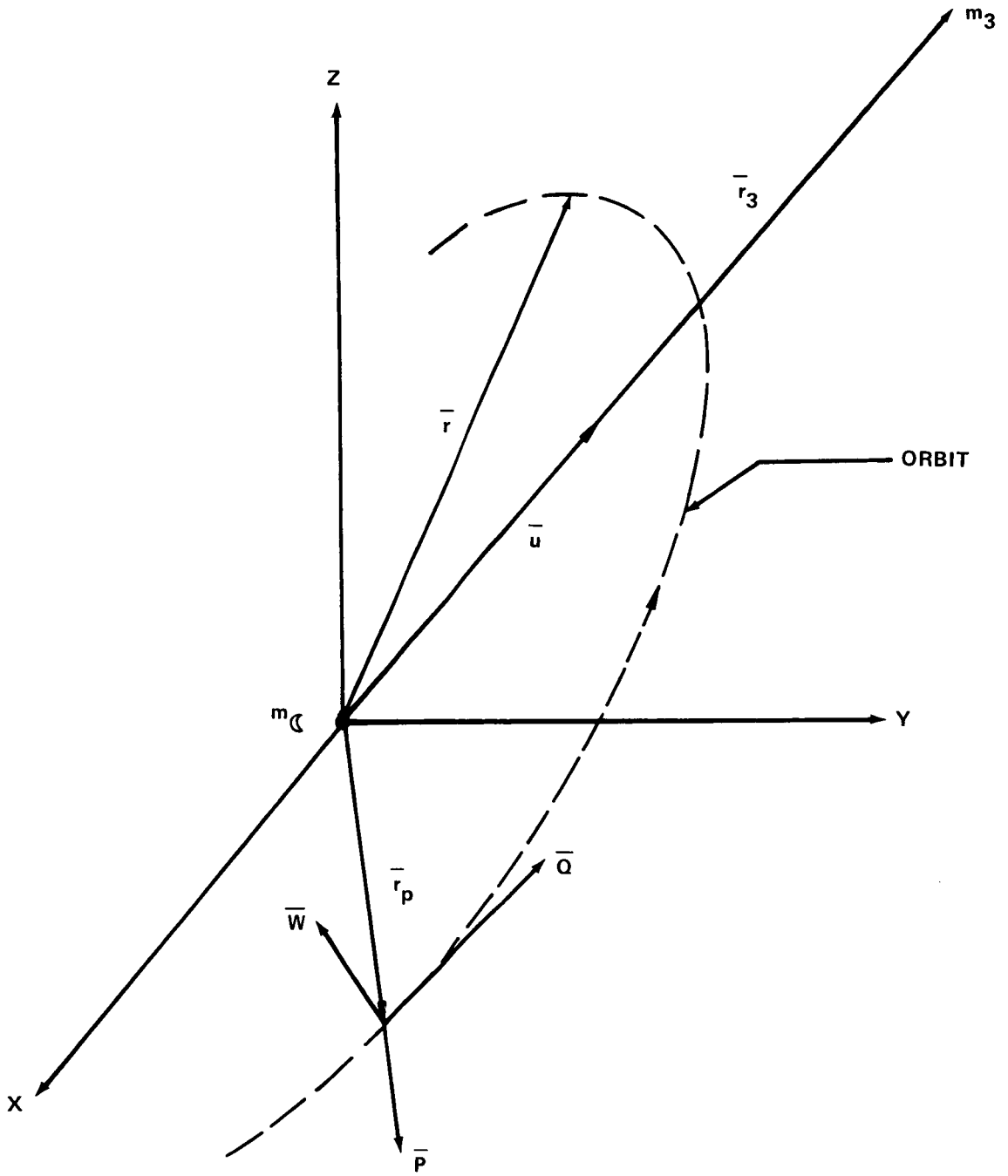

m_3 THIRD BODY MASS

FIGURE 1 - THIRD BODY LOCATION

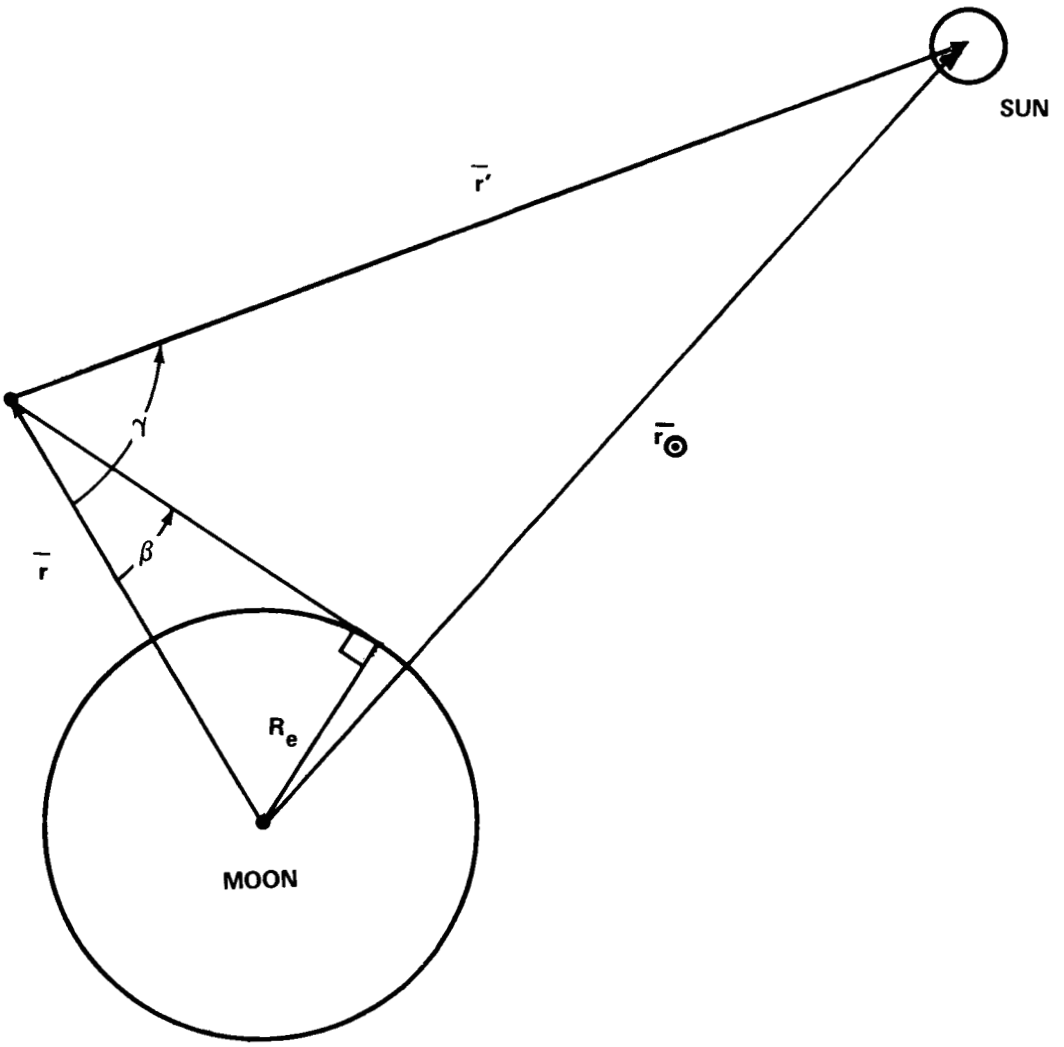

FIGURE 2 - SATELLITE SUN GEOMETERY

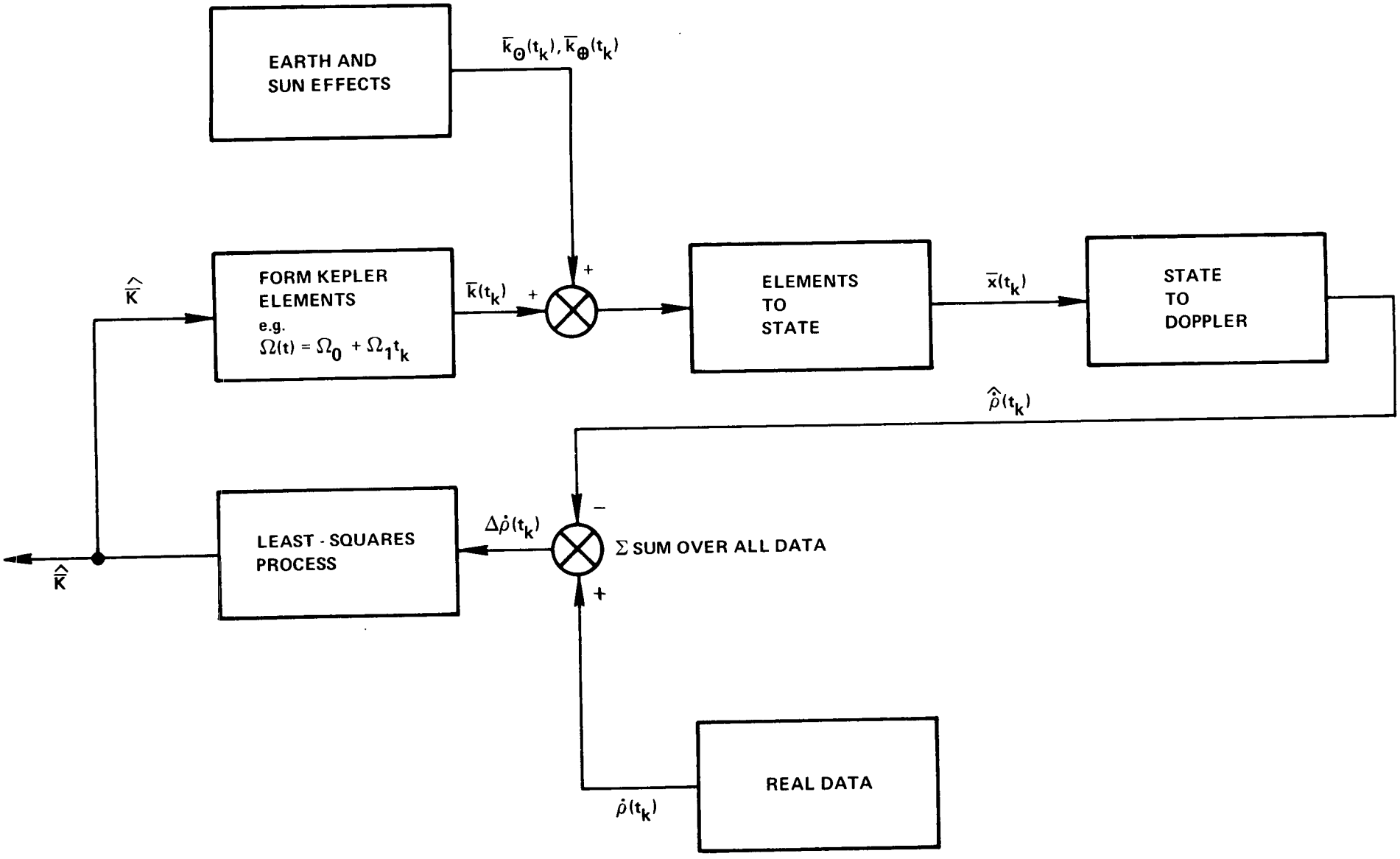

FIGURE 3 - EMPIRICAL ORBIT DETERMINATION BLOCK DIAGRAM

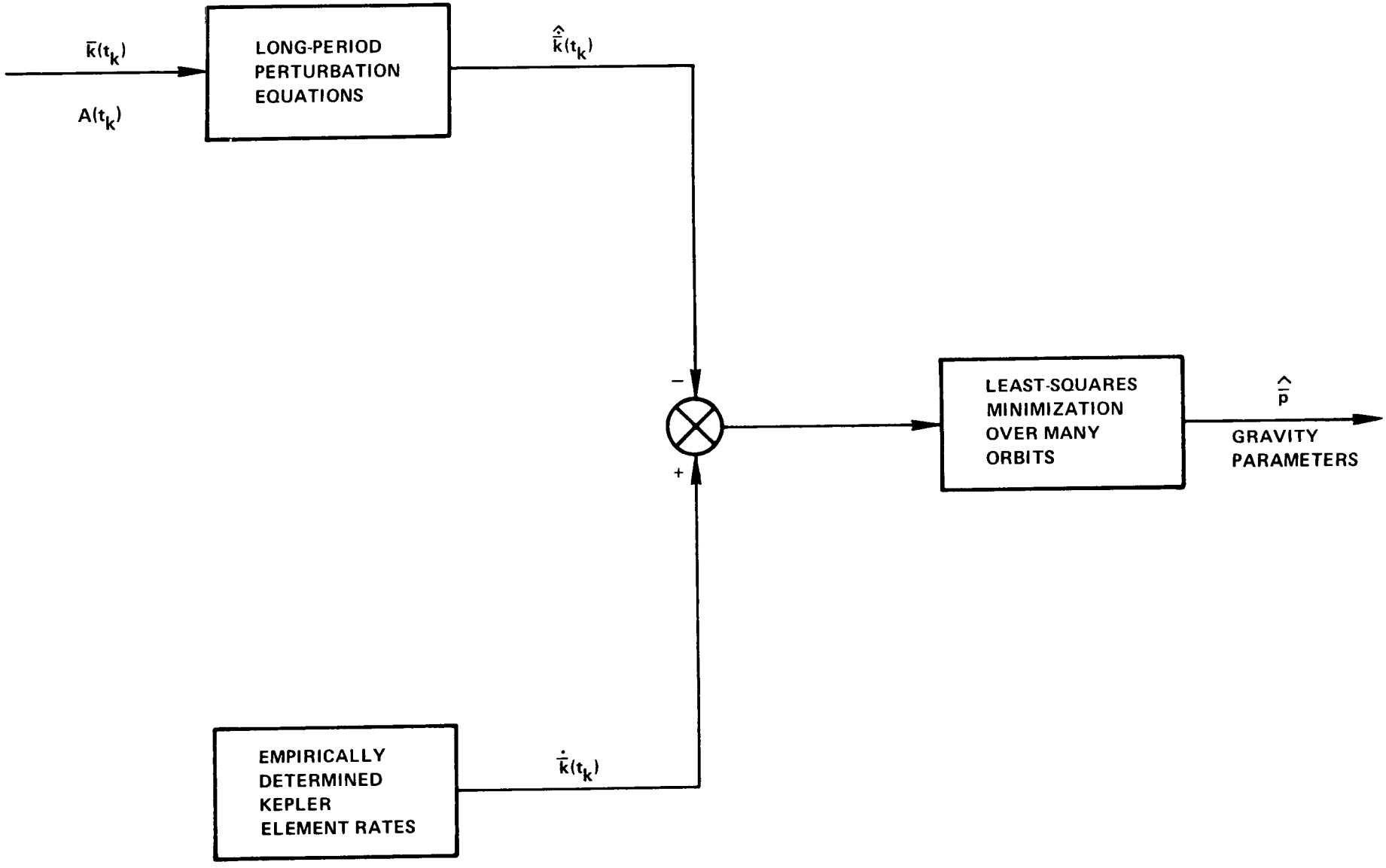

FIGURE 4 - GRAVITY COEFFICIENT ESTIMATION

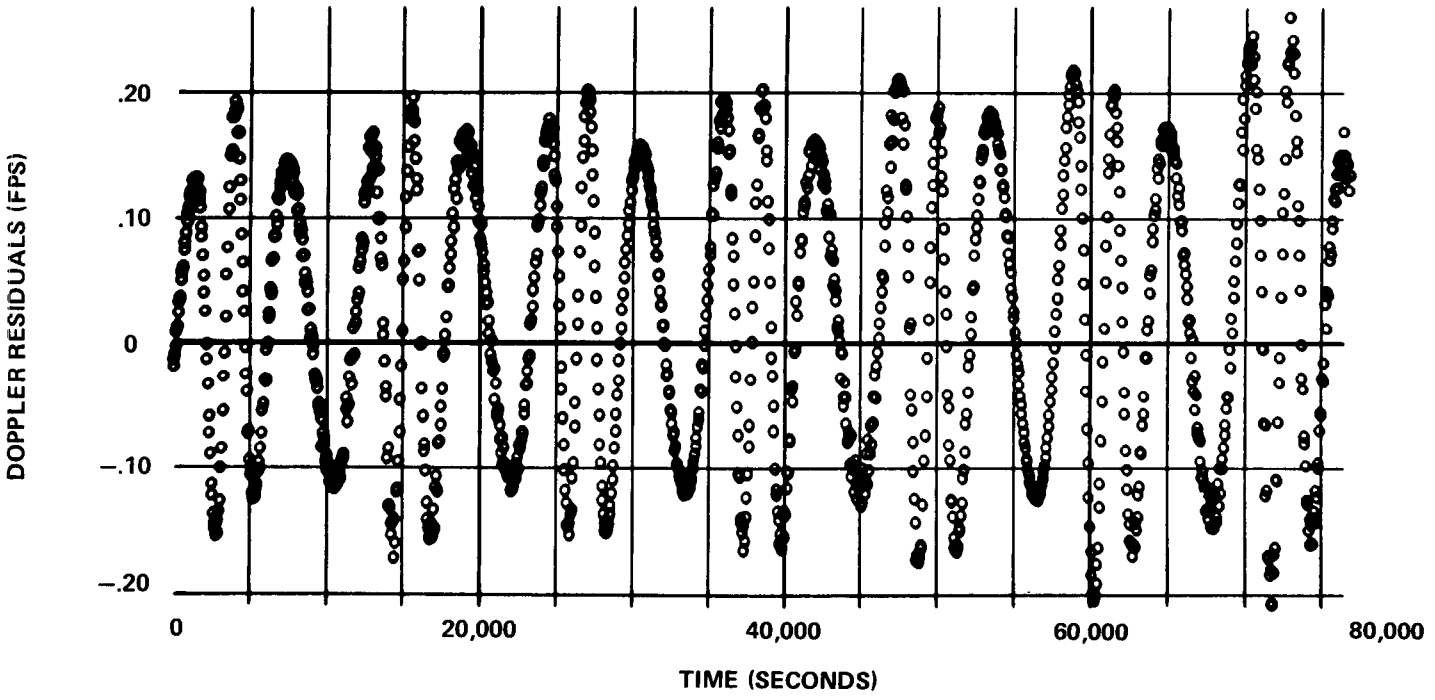

FIGURE 5 - LUNAR ORBITER V PSEUDO DATA RESIDUALS

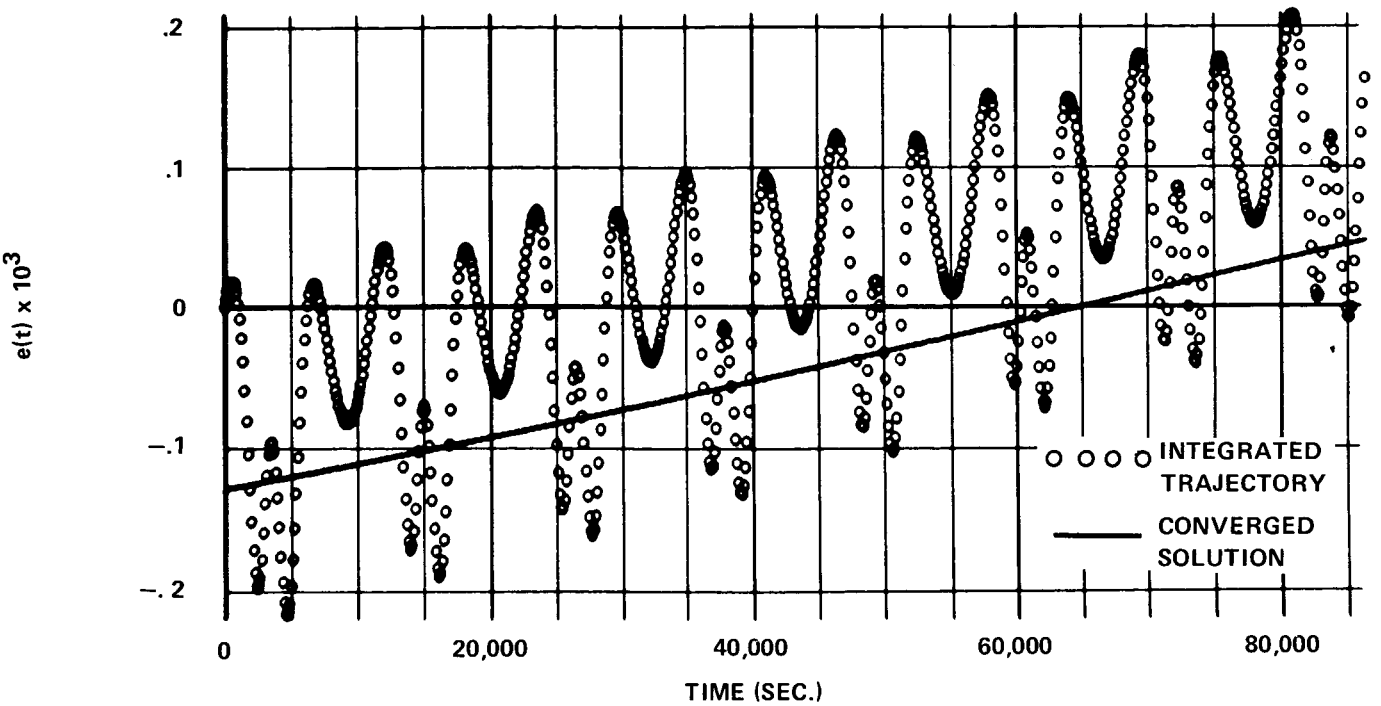

ECCENTRICITY AS A FUNCTION OF TIME
MINUS EPOCH VALUE

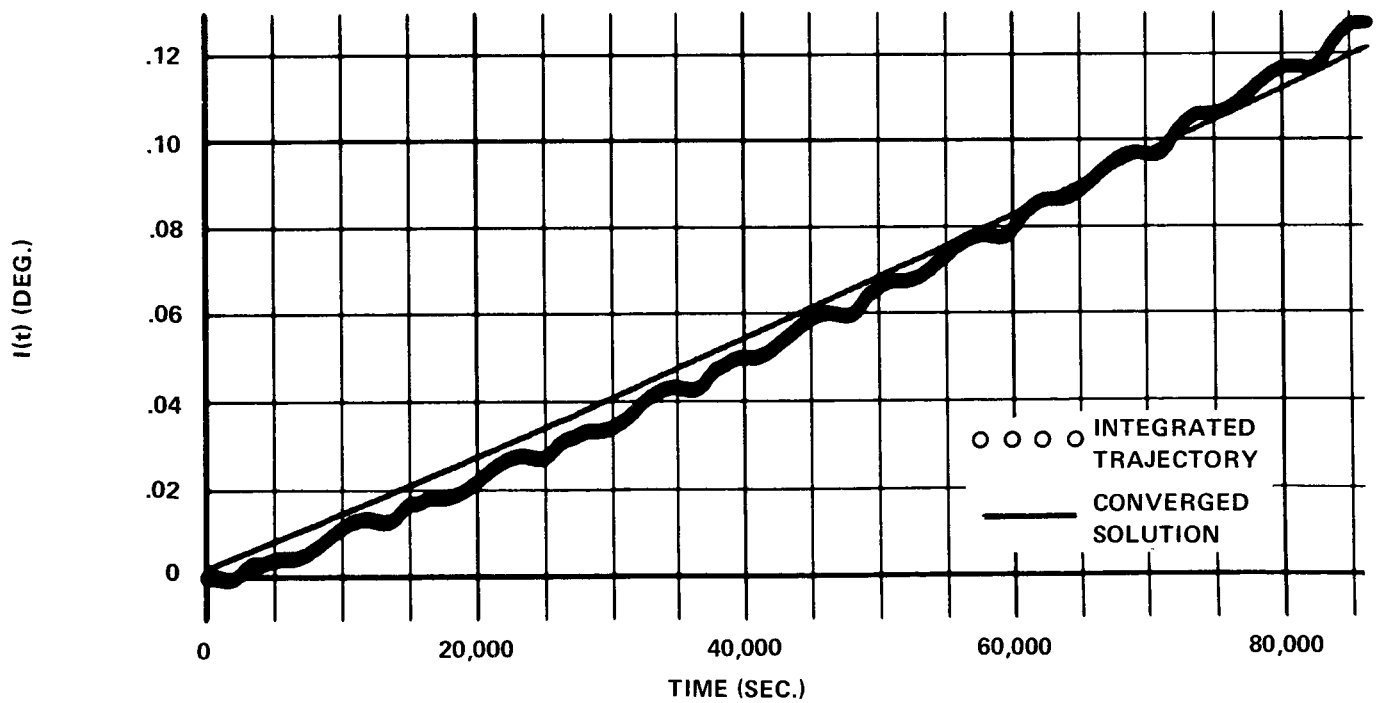

INCLINATION AS A FUNCTION OF TIME
MINUS EPOCH VALUE

FIGURE 6 - LUNAR ORBITER V ORBIT

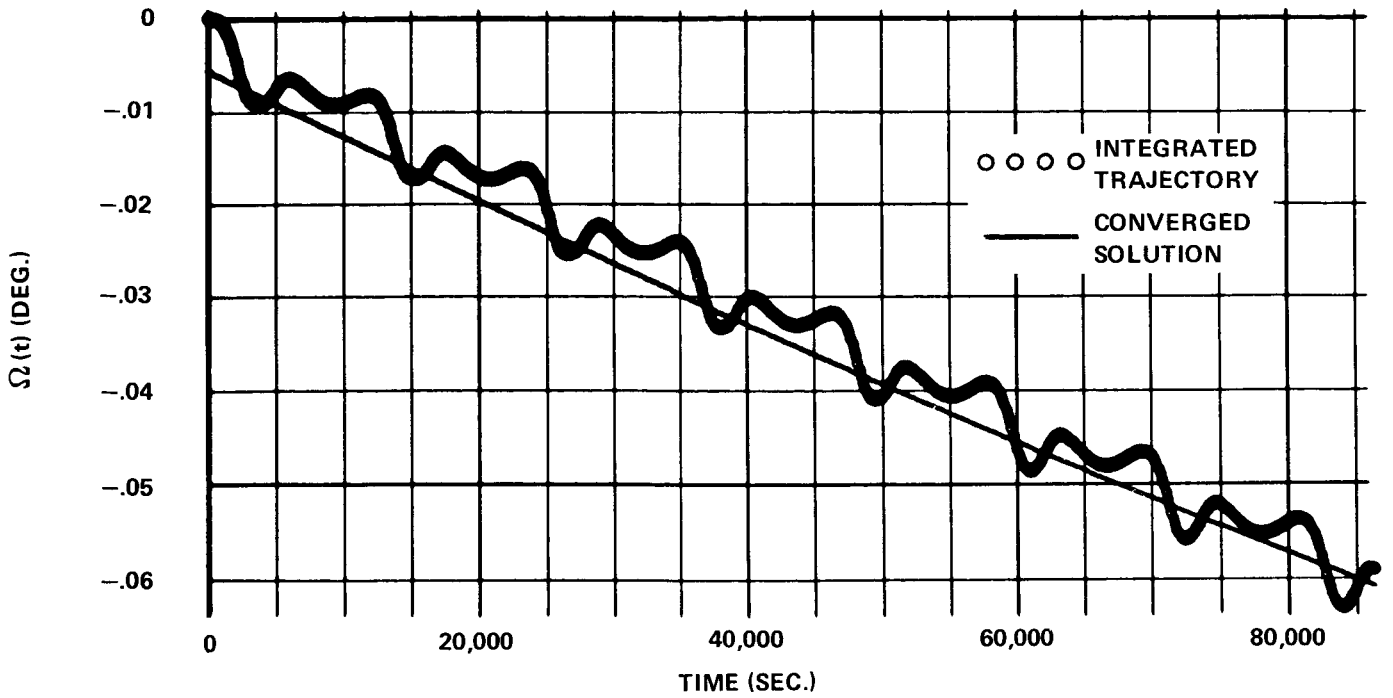

ASCENDING NODE AS A FUNCTION OF TIME
MINUS EPOCH VALUE

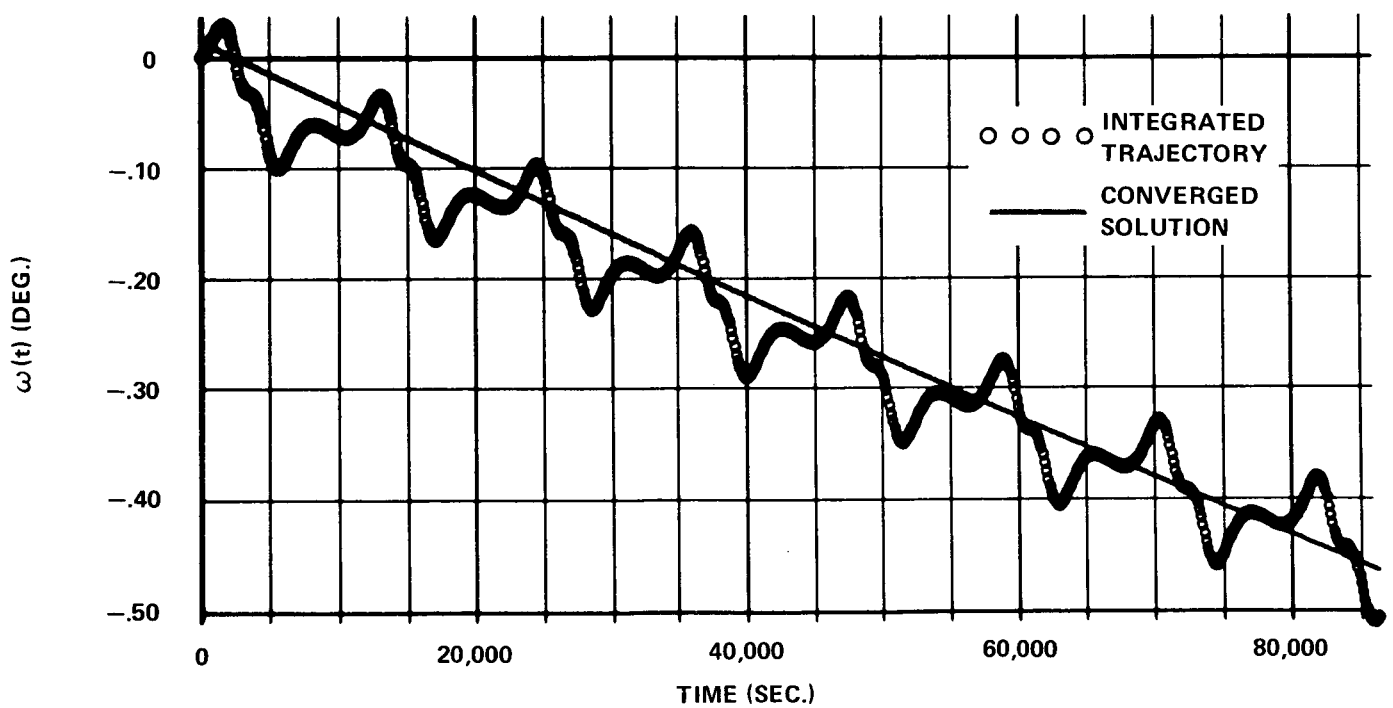

PERIFOCUS AS A FUNCTION OF TIME
MINUS EPOCH VALUE

FIGURE 7 - LUNAR ORBITER V ORBIT

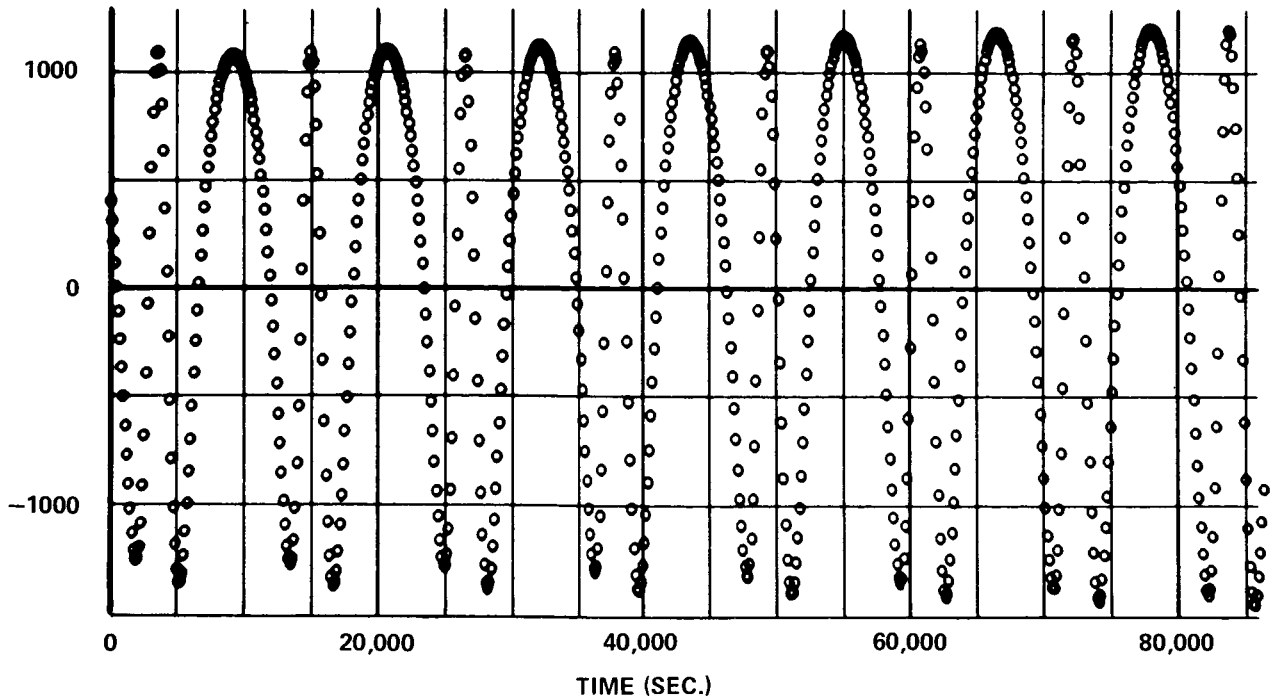

SEMI-MAJOR AXIS DIFFERENCE

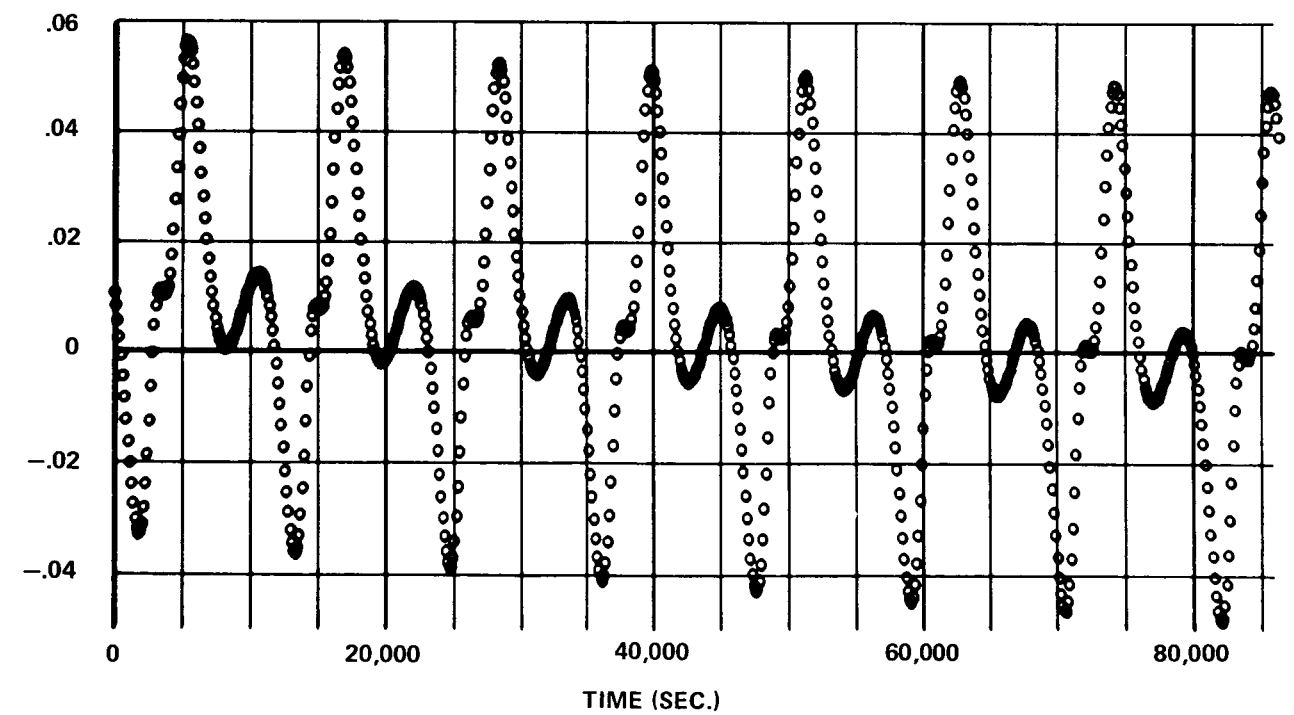

MEAN ANOMALY DIFFERENCE

FIGURE 8 - LUNAR ORBITER V ORBIT

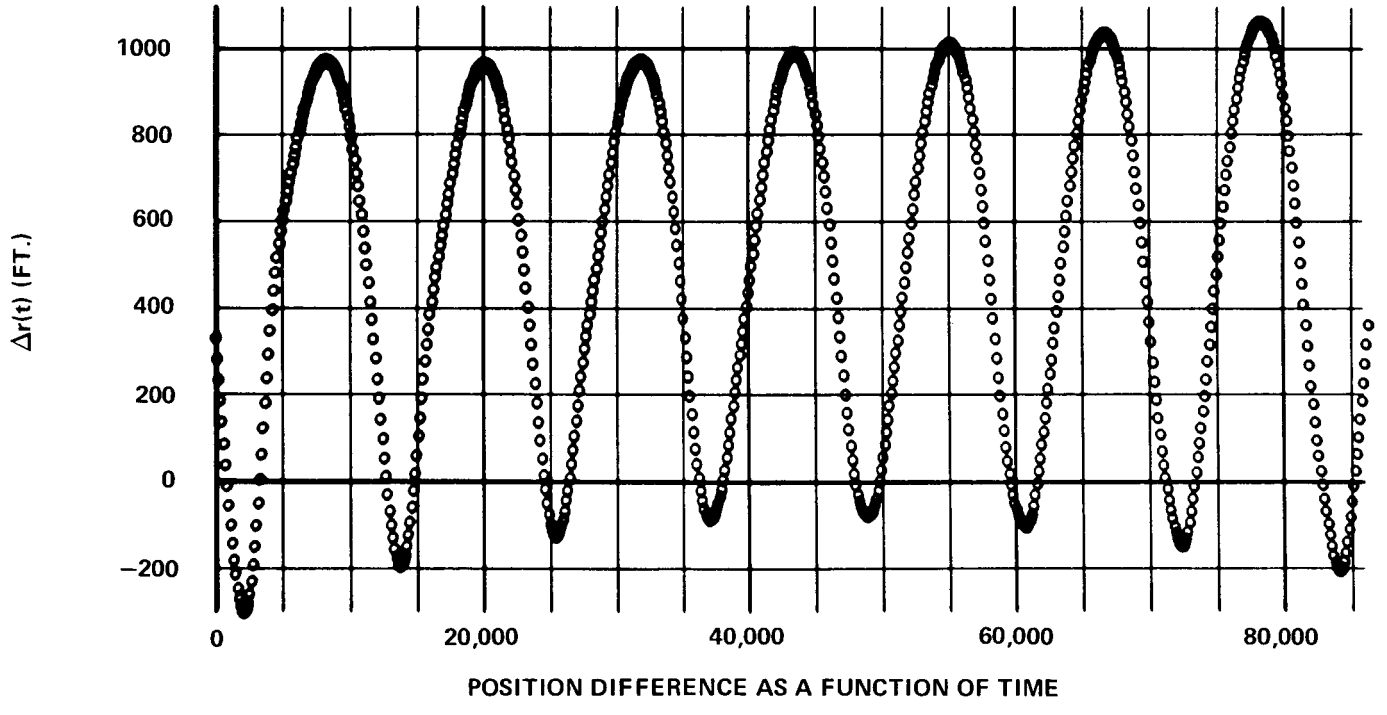

FIGURE 9 - LUNAR ORBITER V ORBIT

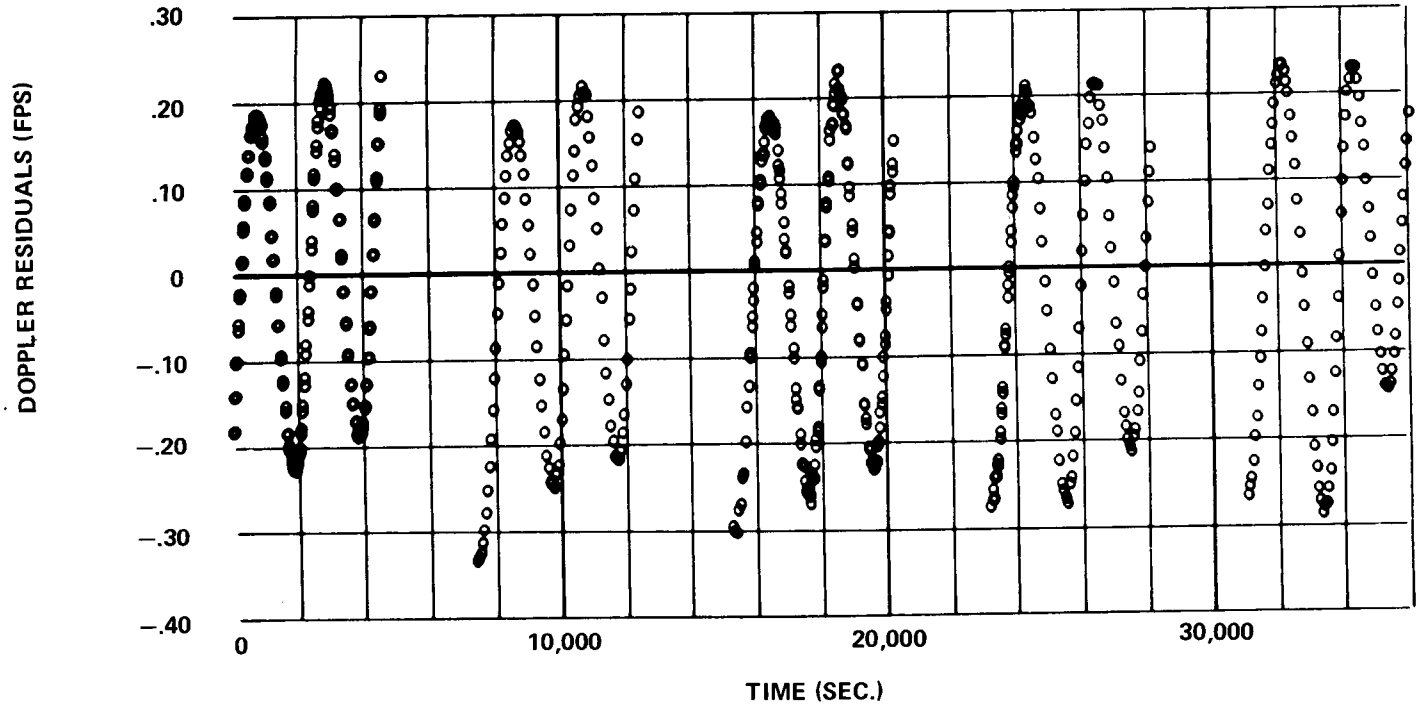

FIGURE 10 - LUNAR ORBITER III PSEUDO DATA DOPPLER RESIDUALS

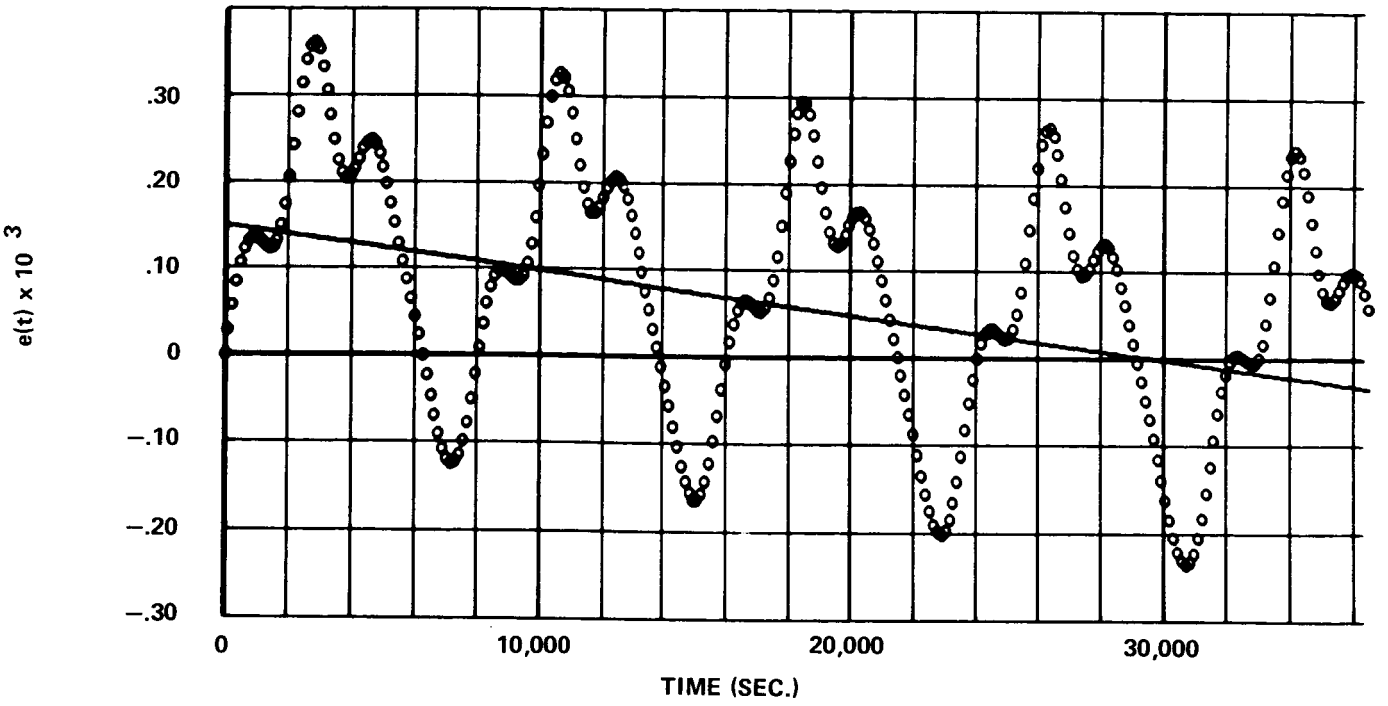

VARIATION IN ECCENTRICITY AS A FUNCTION OF TIME MINUS EPOCH VALUE

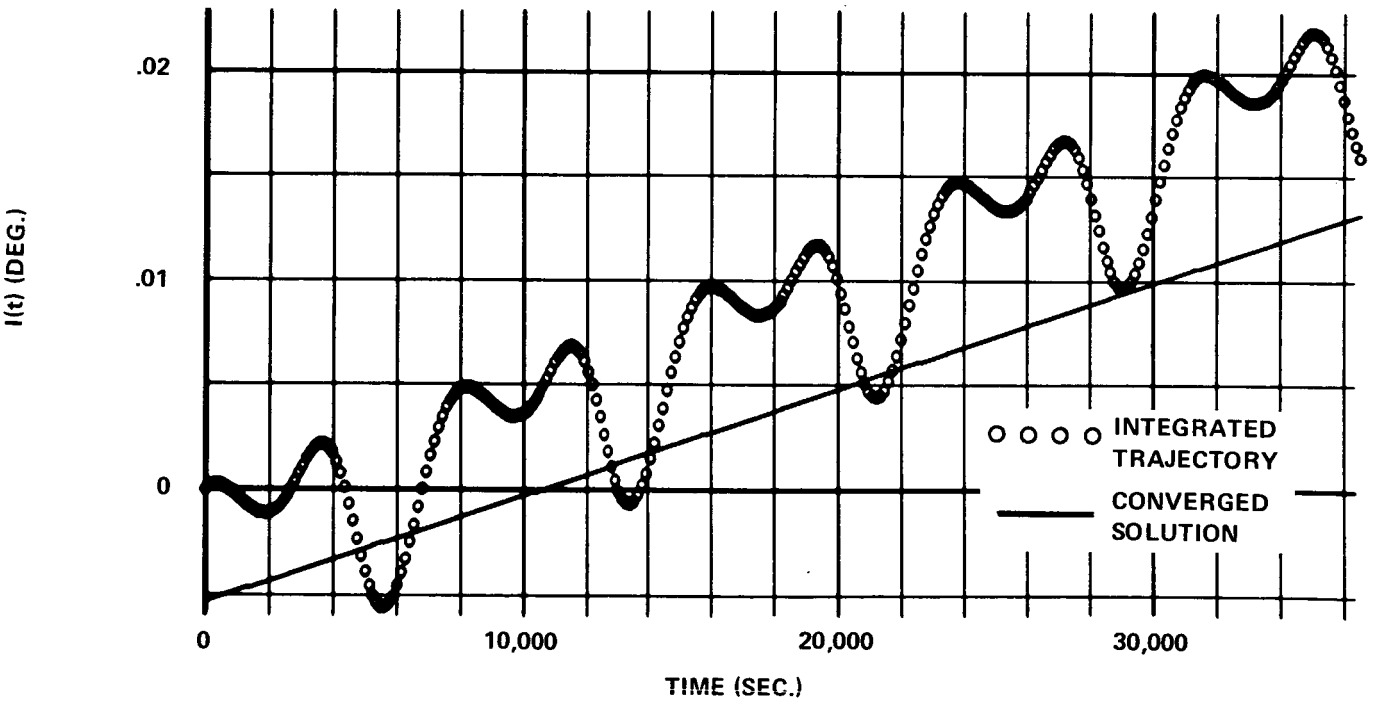

VARIATION IN INCLINATION AS A FUNCTION OF TIME MINUS EPOCH VALUE

FIGURE 11 - LUNAR ORBITER III ORBIT

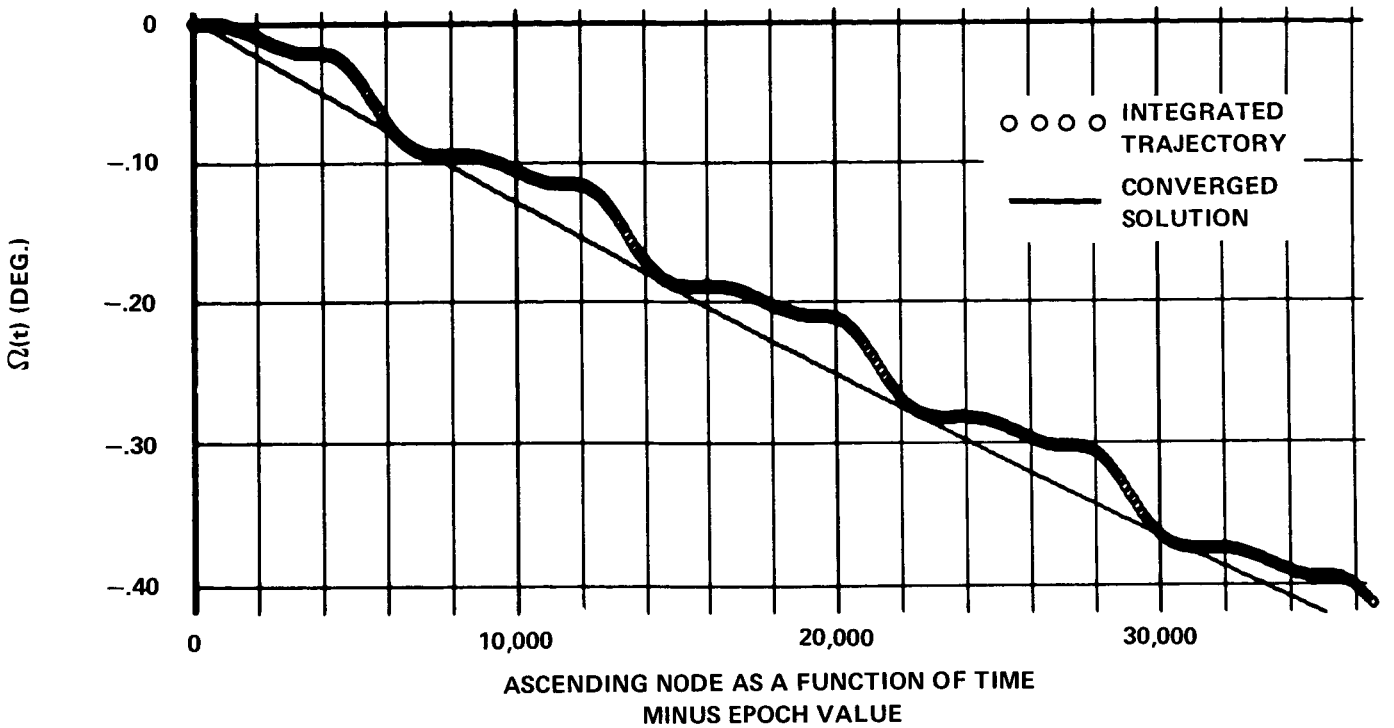

ASCENDING NODE AS A FUNCTION OF TIME
MINUS EPOCH VALUE

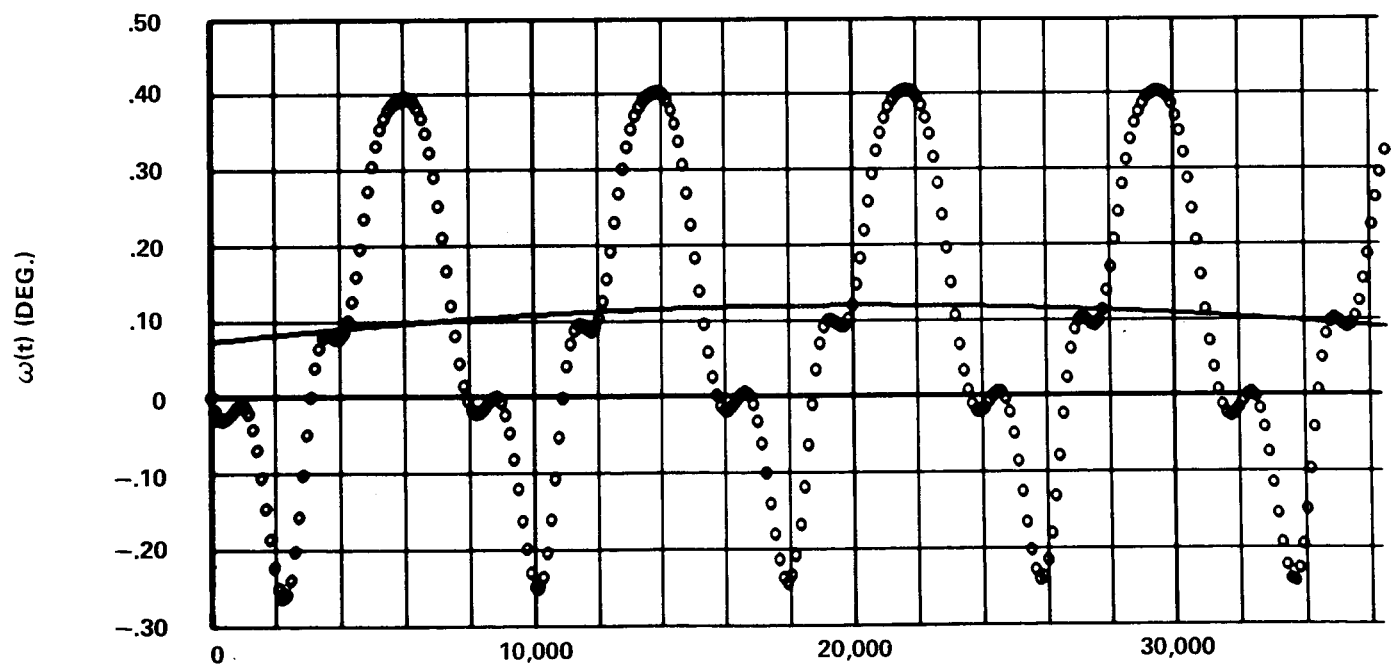

PERIFOCUS AS A FUNCTION OF TIME
MINUS EPOCH VALUE

FIGURE 12 - LUNAR ORBITER III ORBIT

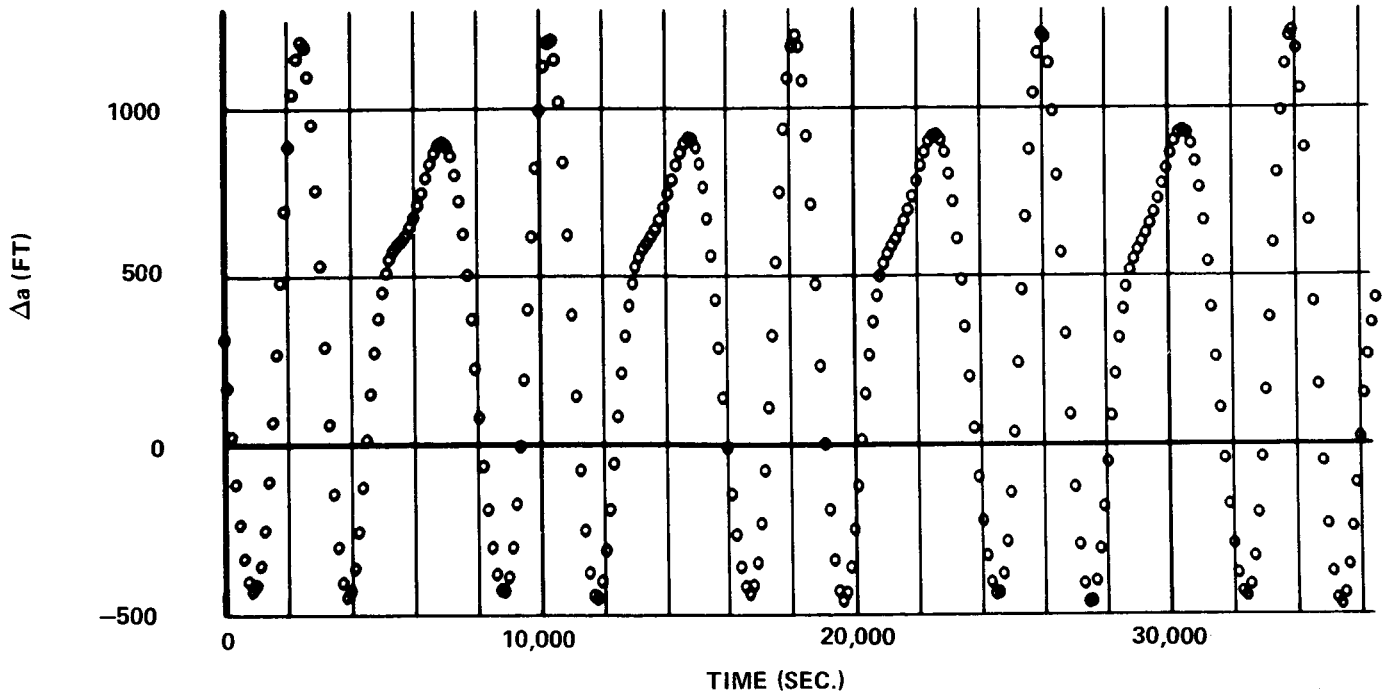

SEMI-MAJOR AXIS DIFFERENCE

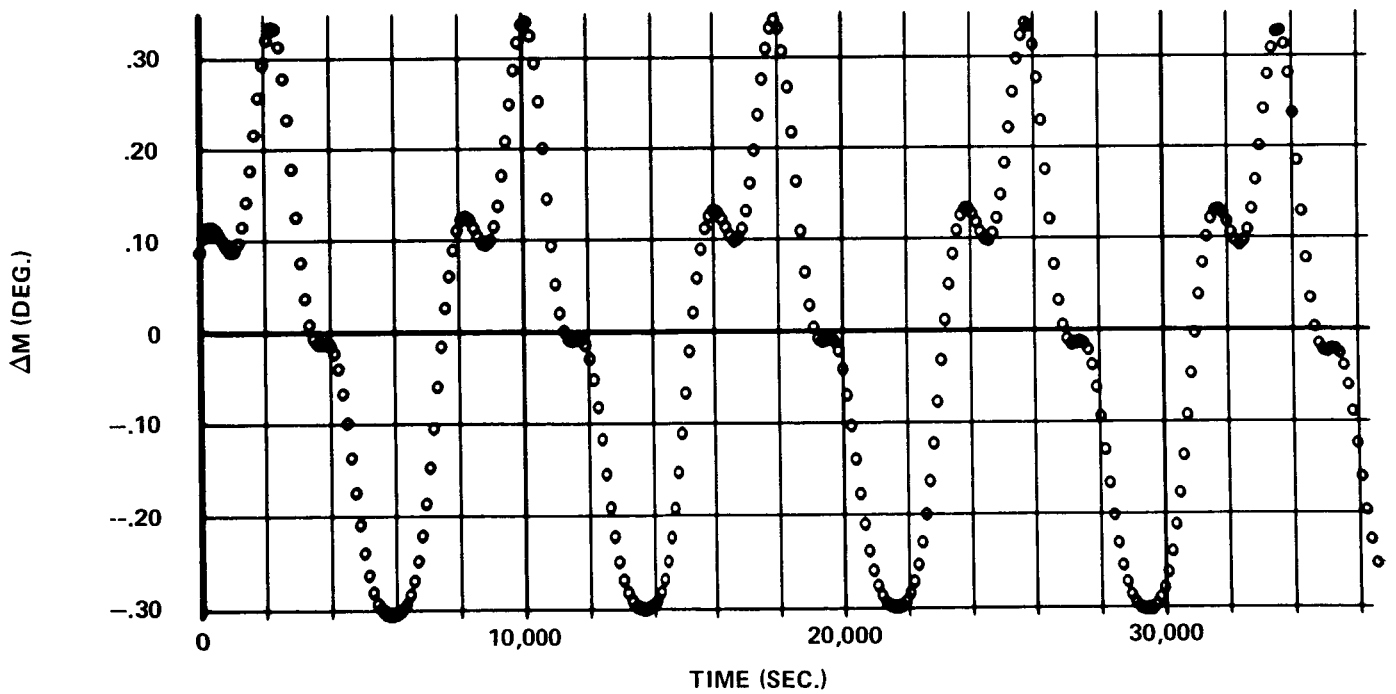

MEAN ANOMALY DIFFERENCE

FIGURE 13 - LUNAR ORBITER III ORBIT

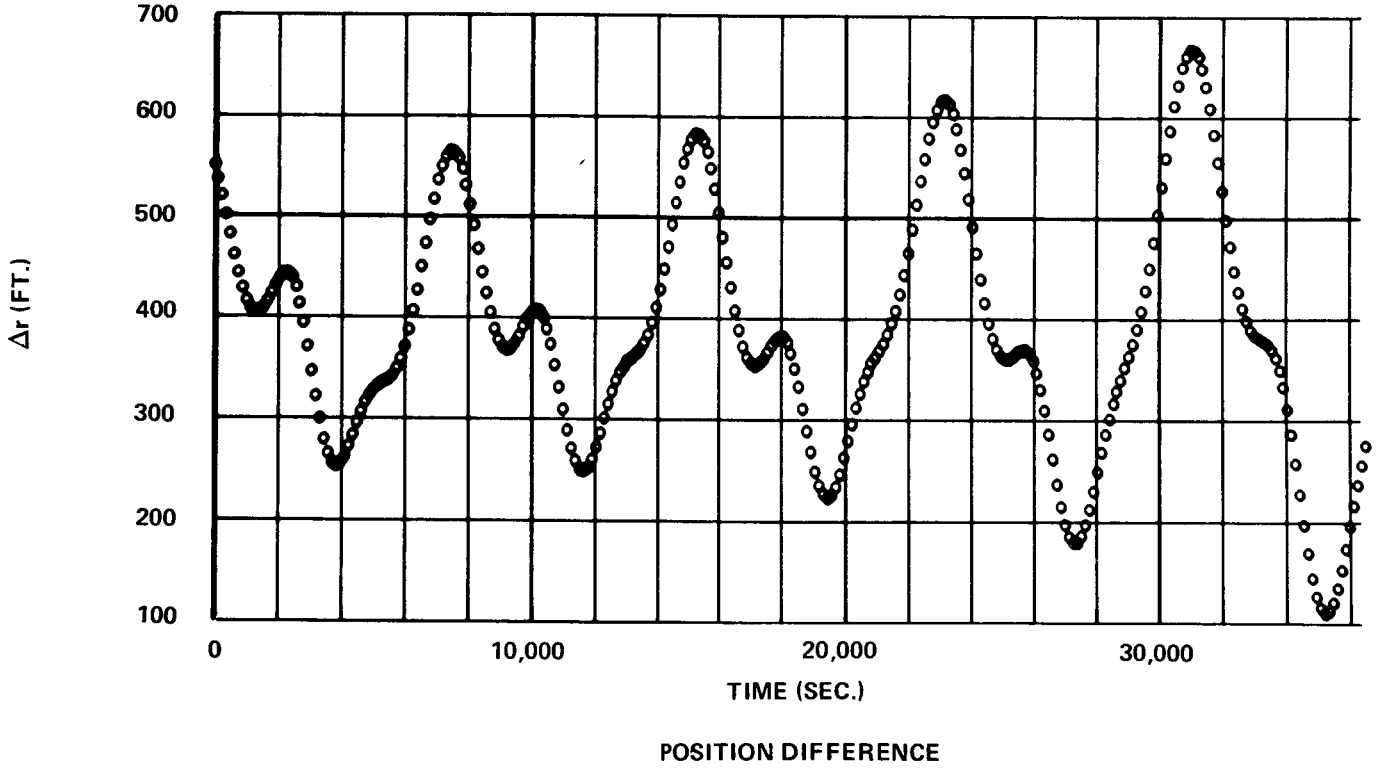

FIGURE 14 - LUNAR ORBITER III ORBIT

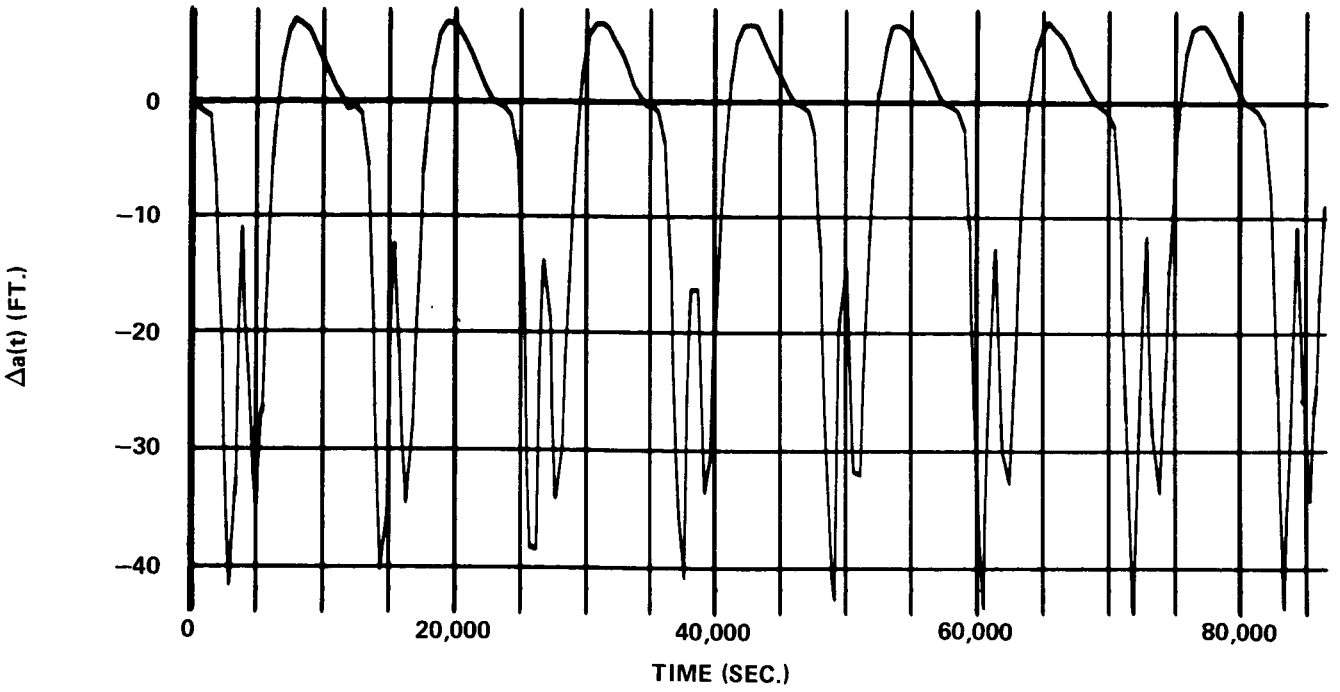

SEMI-MAJOR AXIS DIFFERENCE VS. TIME

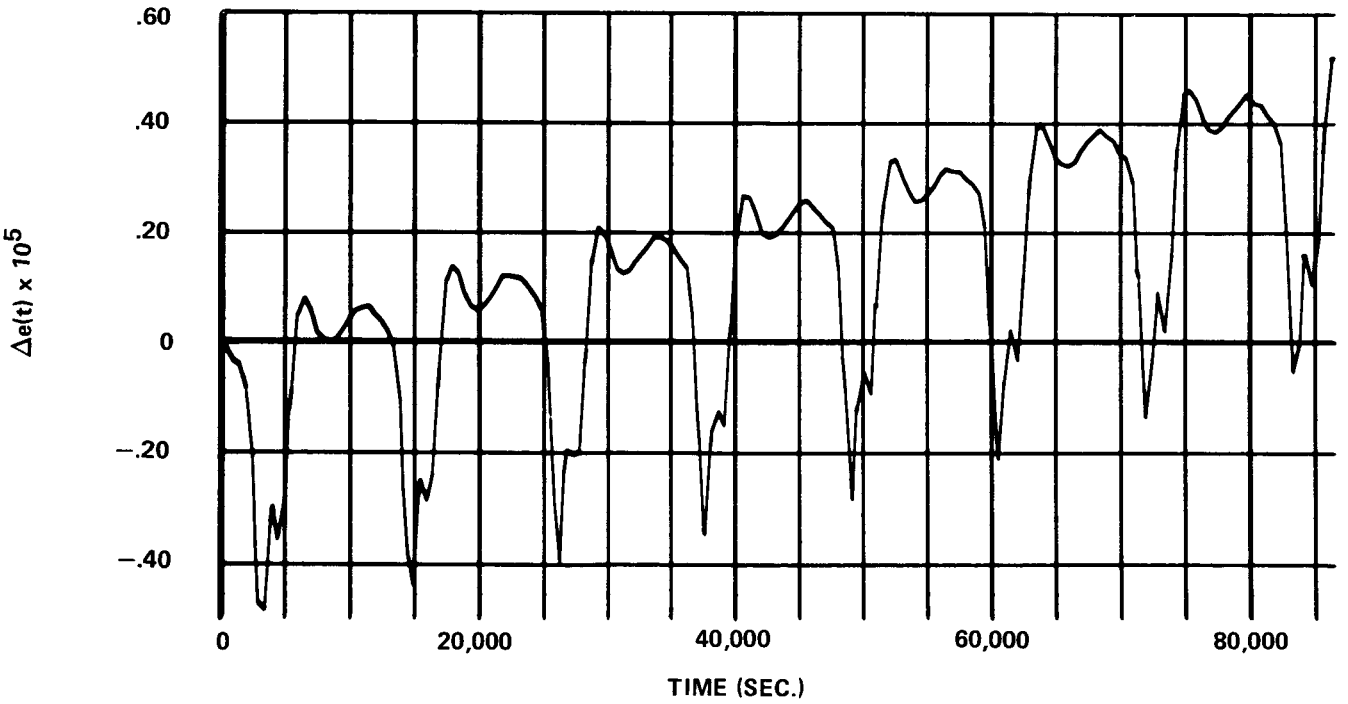

ECCENTRICITY DIFFERENCE VS. TIME

FIGURE 15 - LUNAR ORBITER V ORBIT

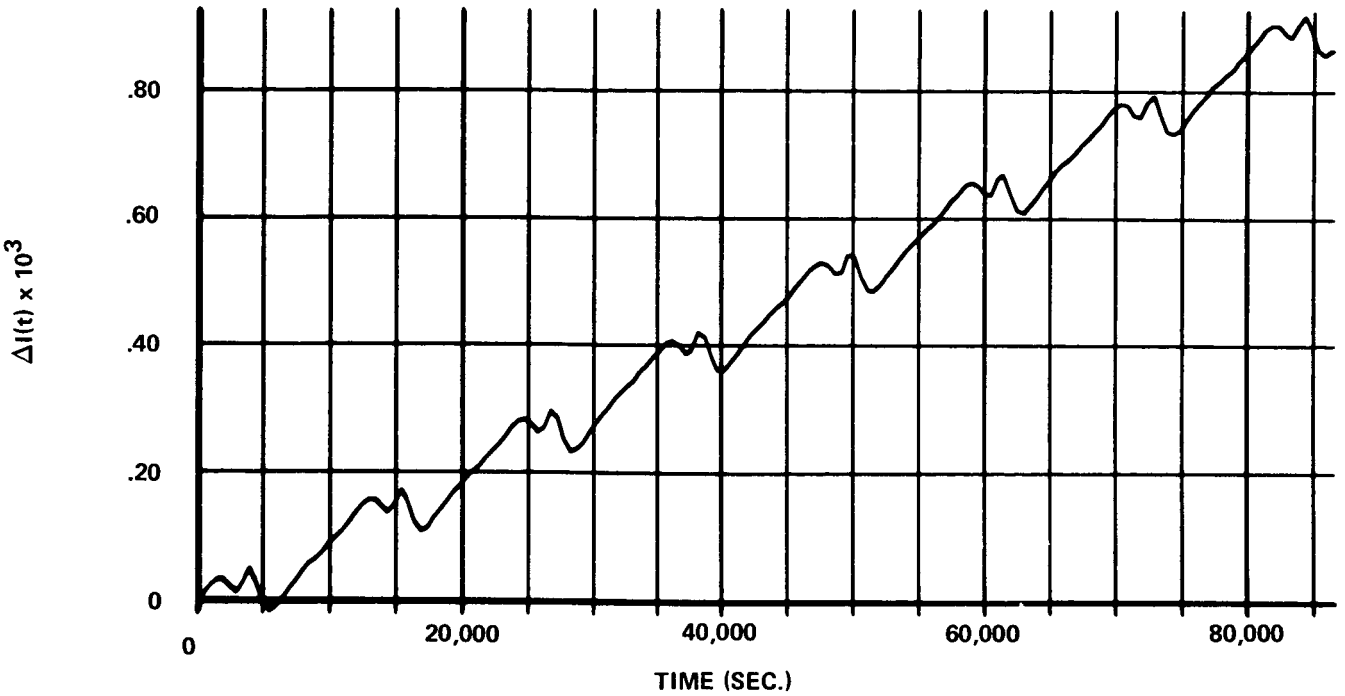

INCLINATION DIFFERENCE VS. TIME

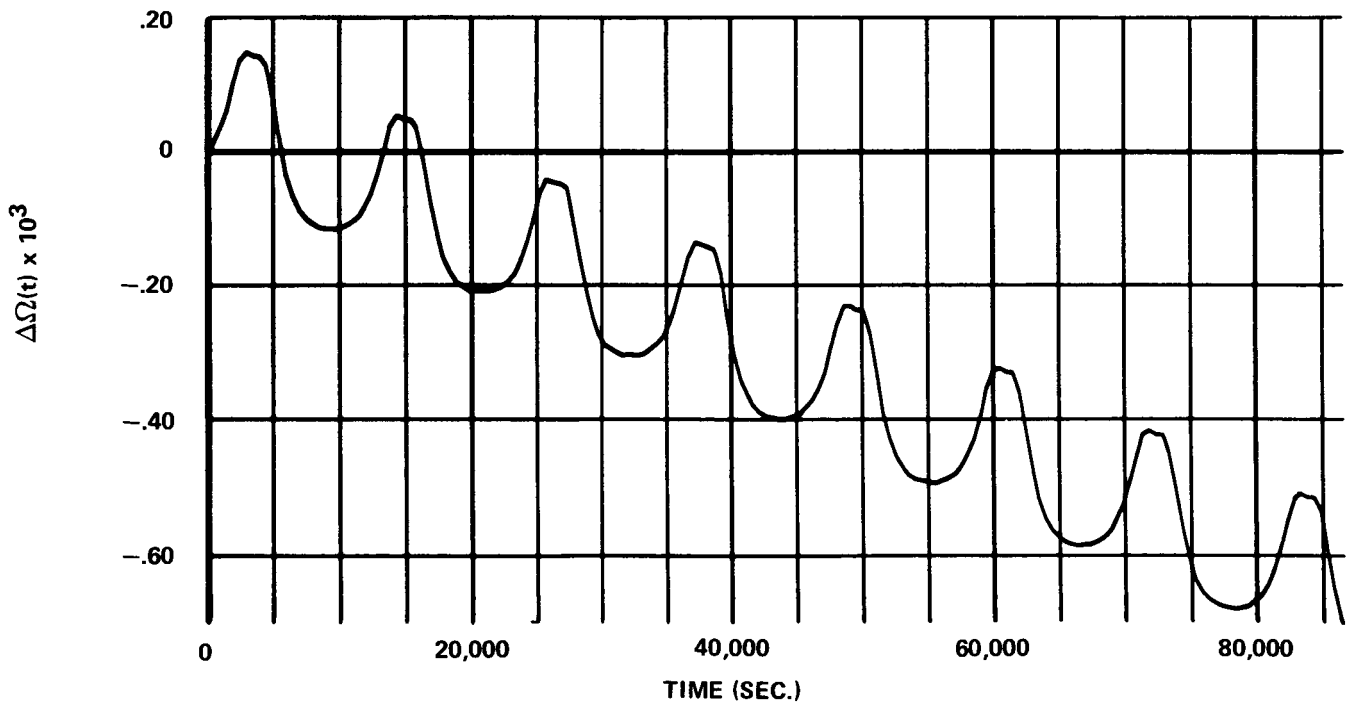

ASCENDING NODE DIFFERENCE VS. TIME

FIGURE 16 - LUNAR ORBITER V ORBIT

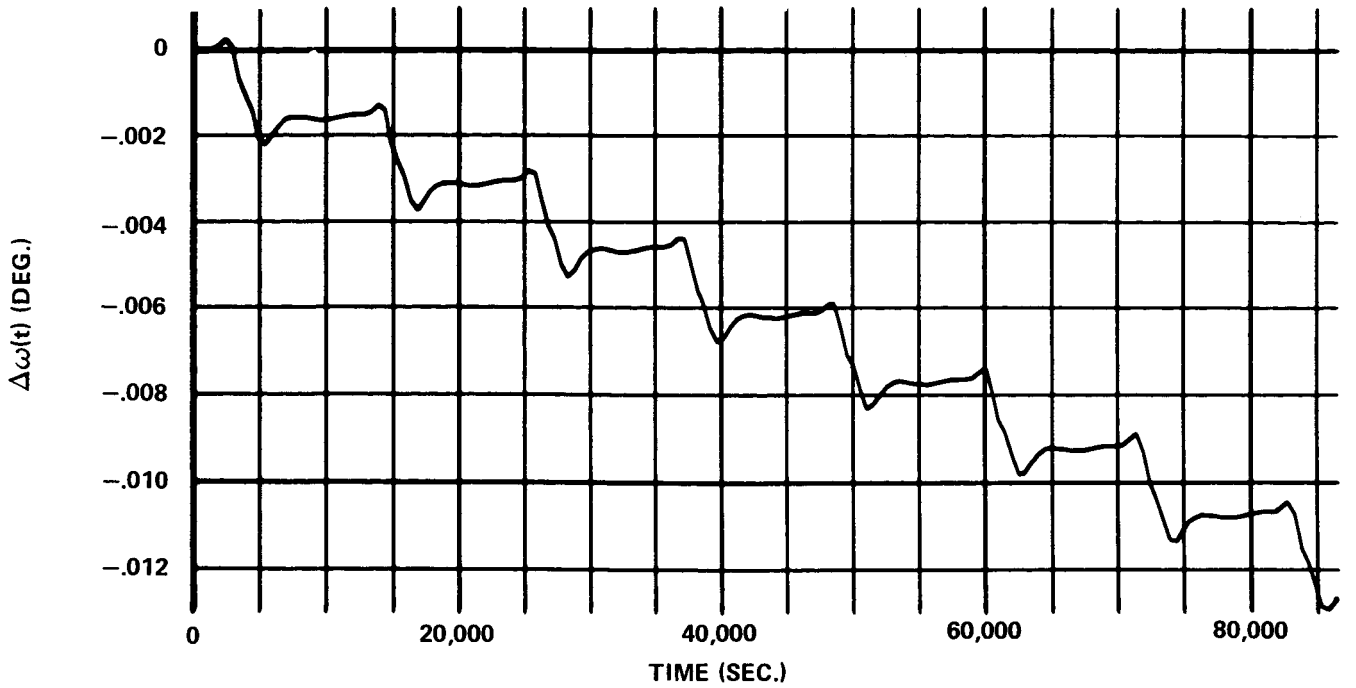

PERIFOCUS DIFFERENCE VS. TIME

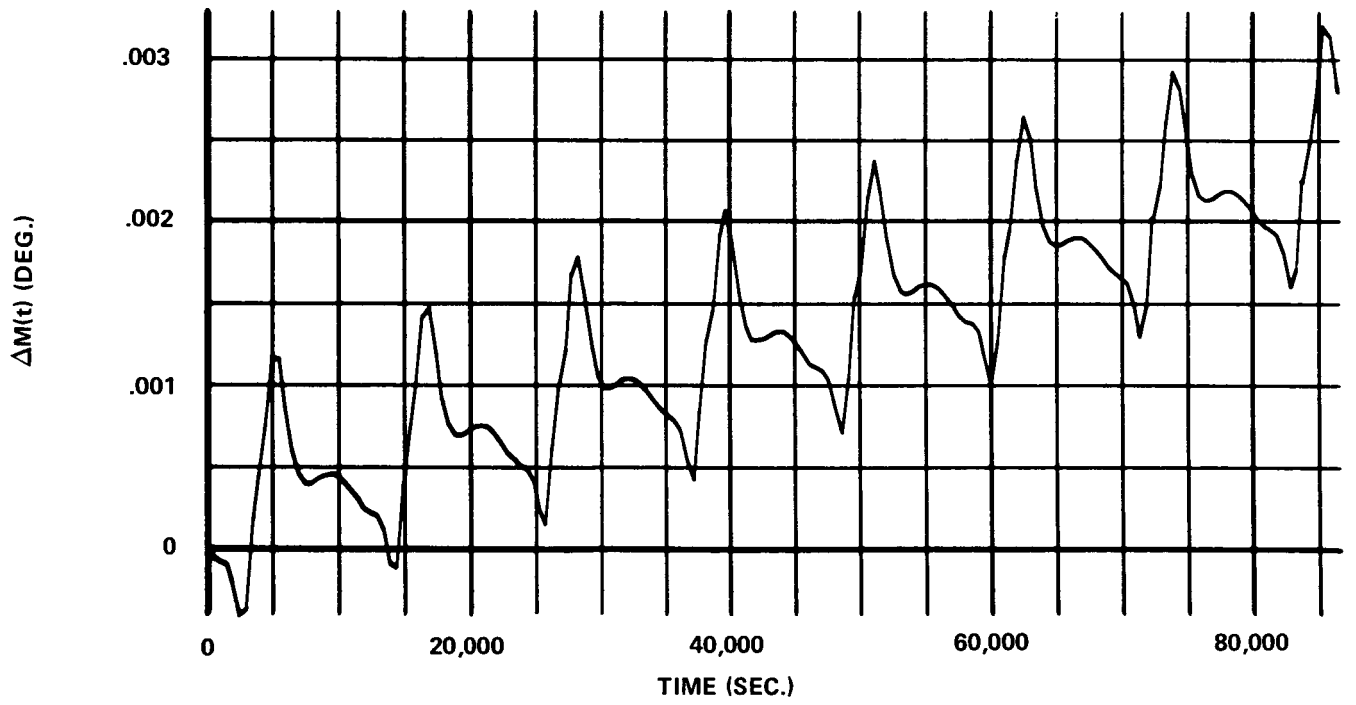

MEAN ANOMALY DIFFERENCE VS. TIME

FIGURE 17 - LUNAR ORBITER V ORBIT

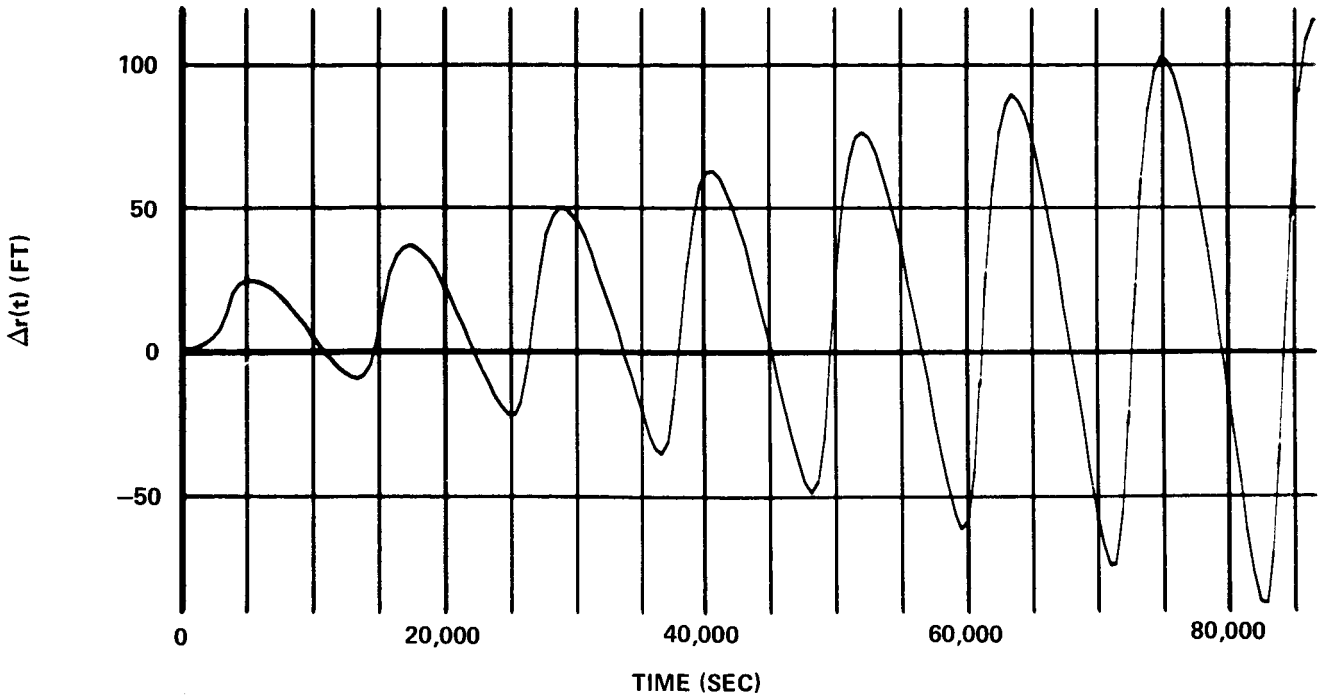

POSITION DIFFERENCE VS. TIME

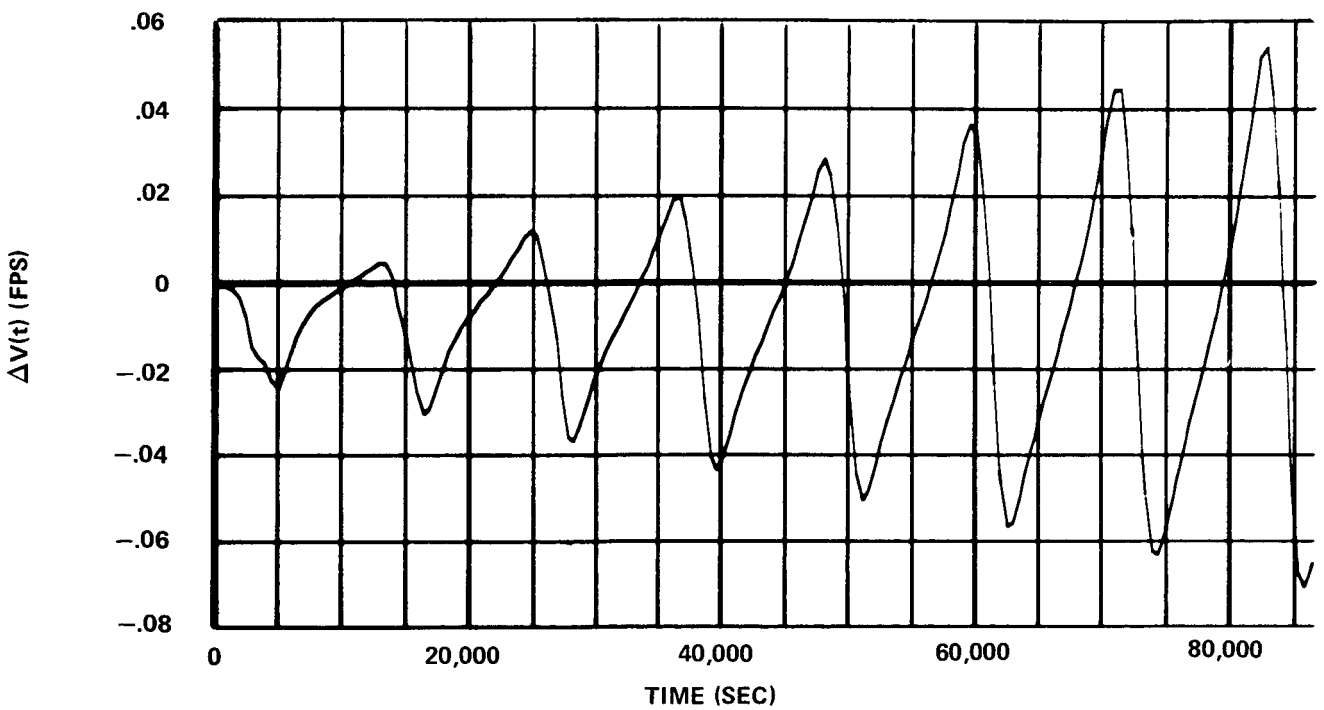

VELOCITY DIFFERENCE VS TIME

FIGURE 18 - LUNAR ORBITER V ORBIT

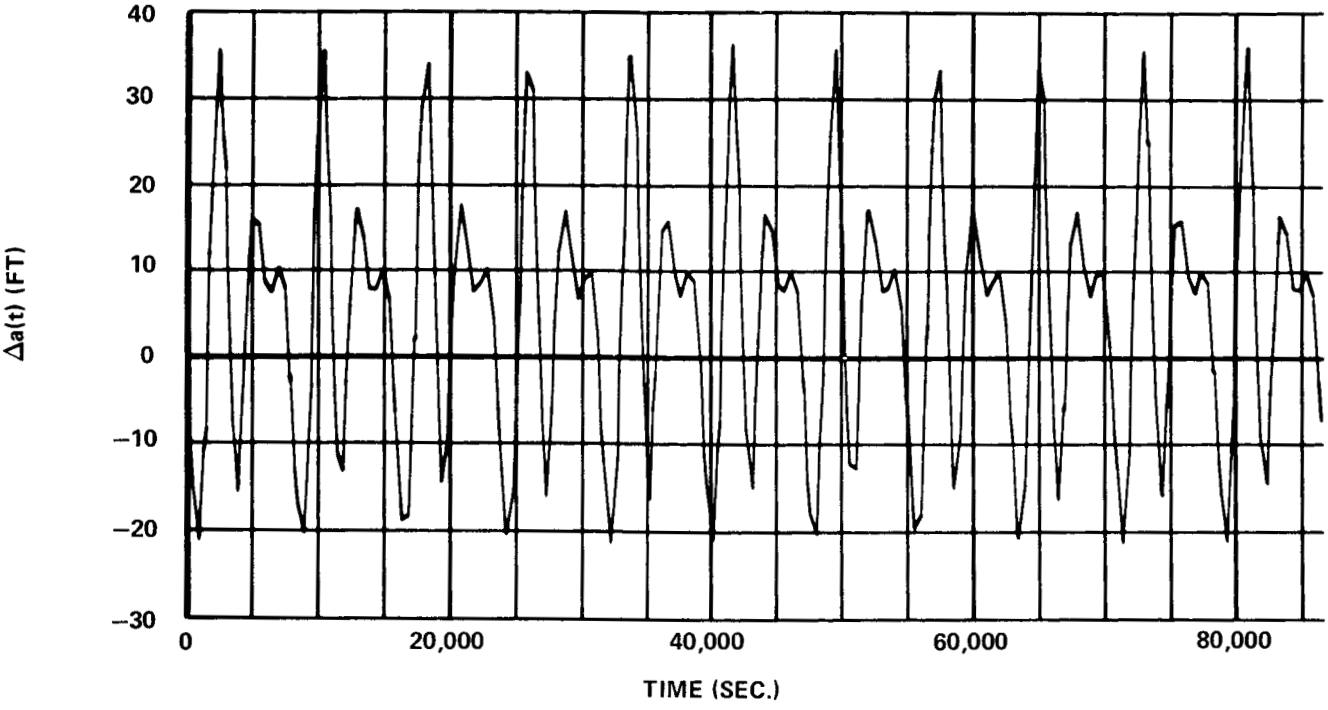

SEMI-MAJOR AXIS DIFFERENCE VS. TIME

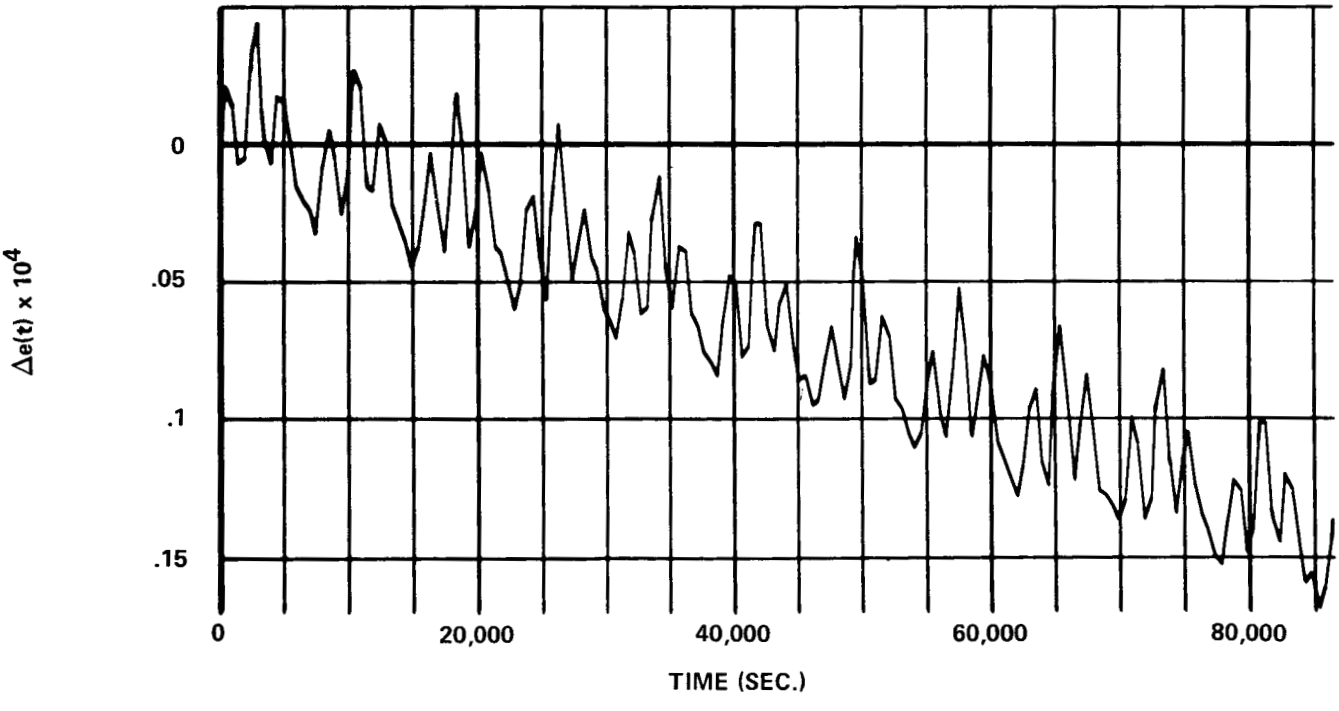

ECCENTRICITY DIFFERENCE VS. TIME

FIGURE 19 - LUNAR ORBITER III ORBIT

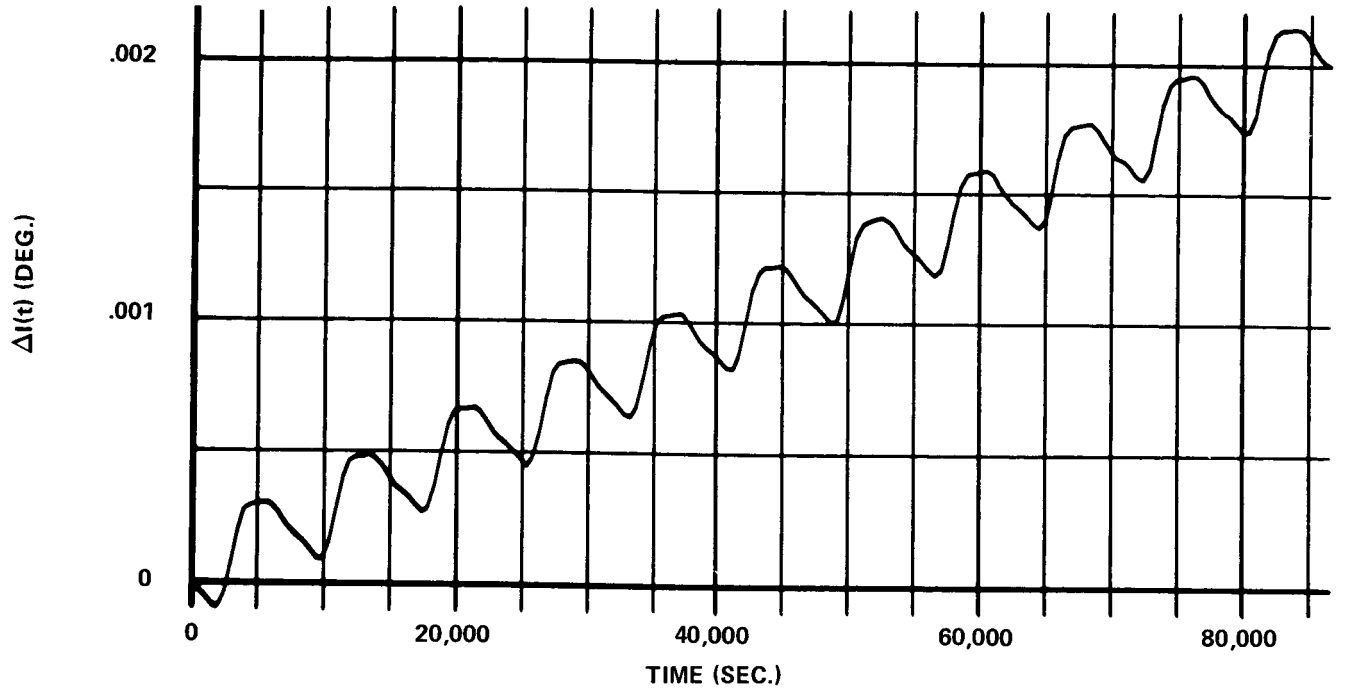

INCLINATION DIFFERENCE VS. TIME

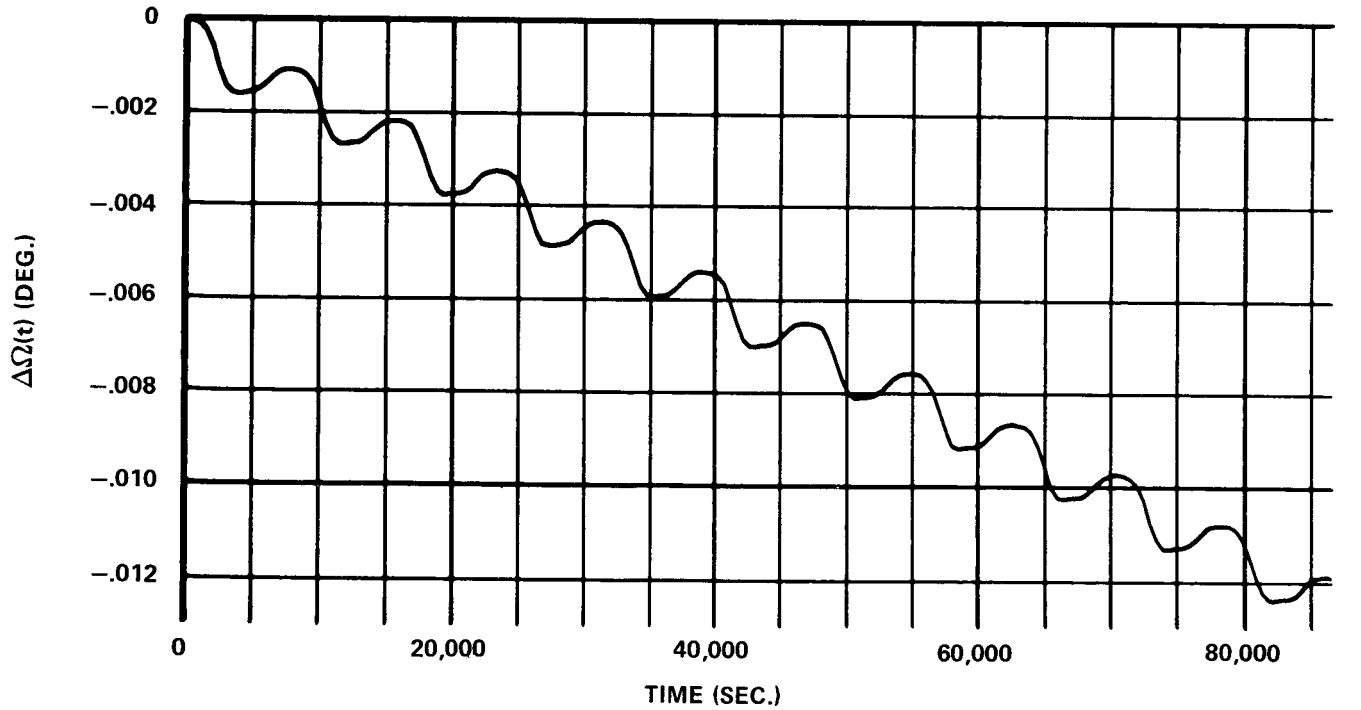

ASCENDING NODE DIFFERENCE VS. TIME

FIGURE 20 - LUNAR ORBITER III ORBIT

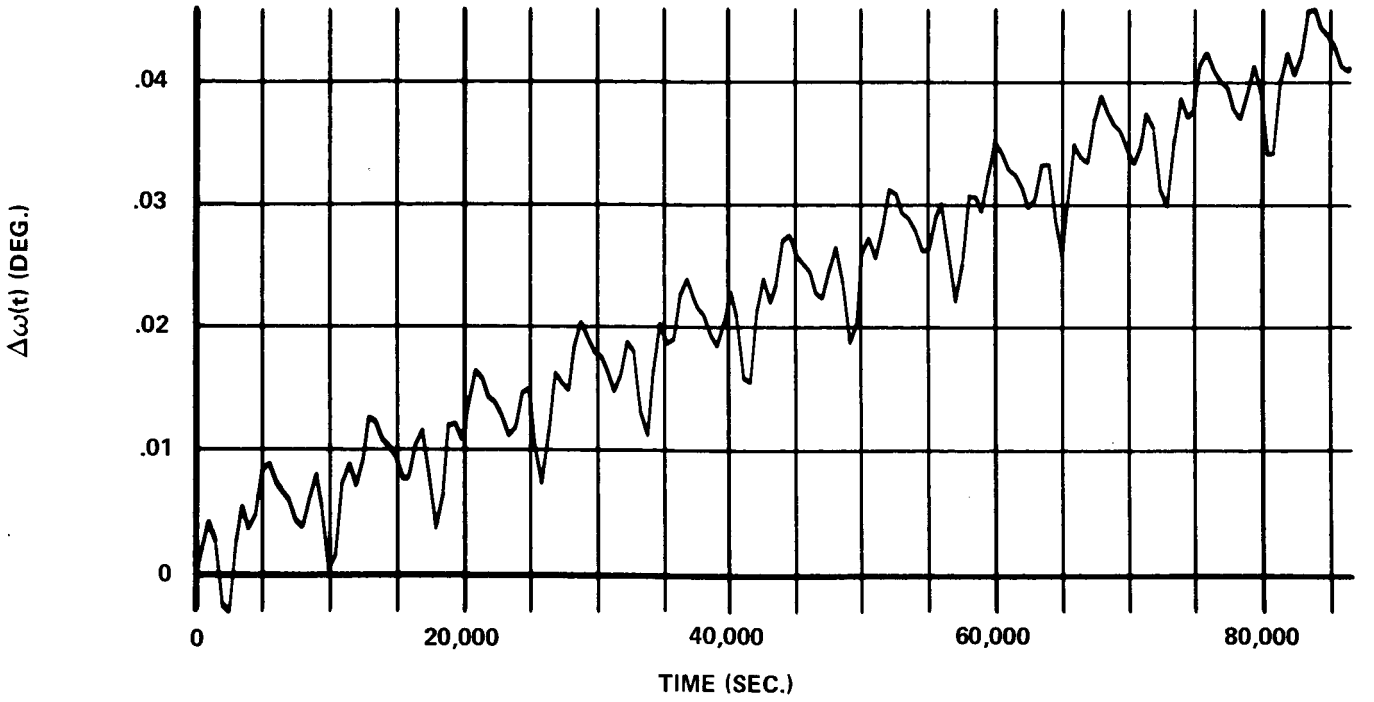

PERIFOCUS DIFFERENCE VS. TIME

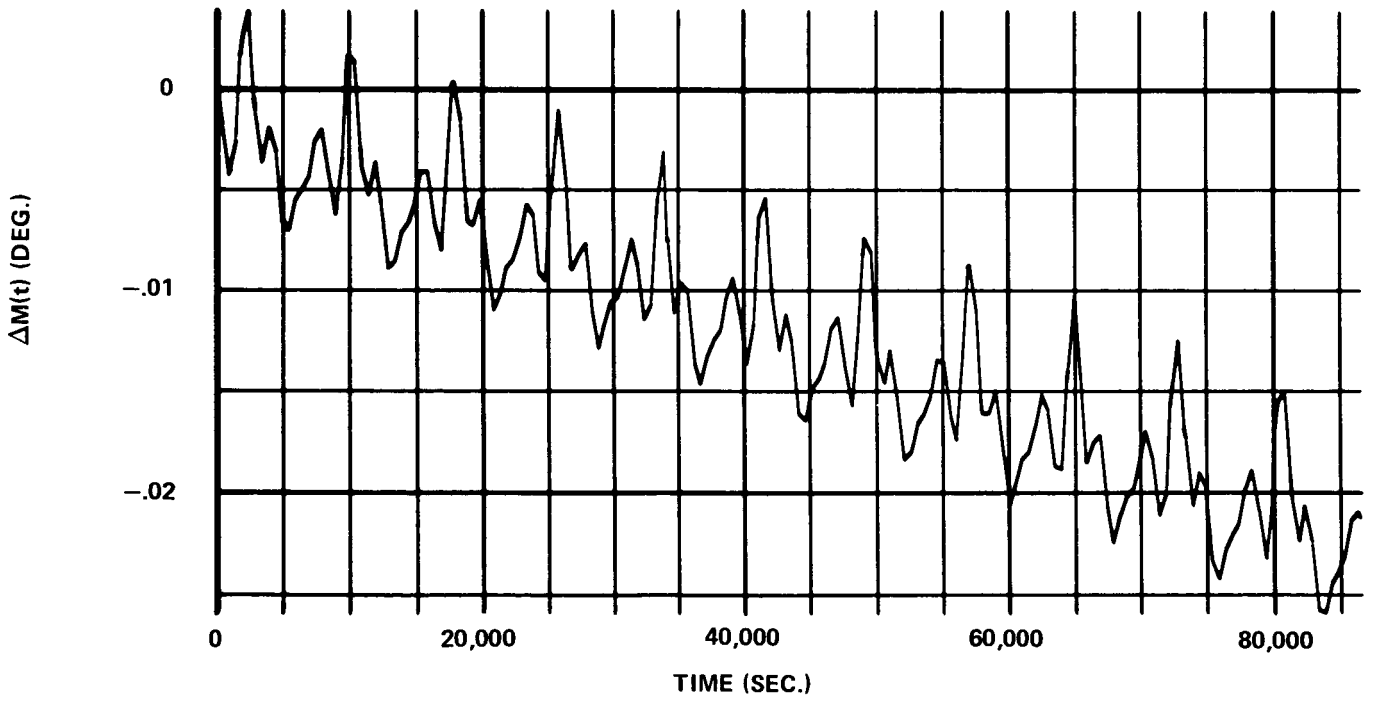

MEAN ANOMALY DIFFERENCE VS. TIME

FIGURE 21 - LUNAR ORBITER III ORBIT

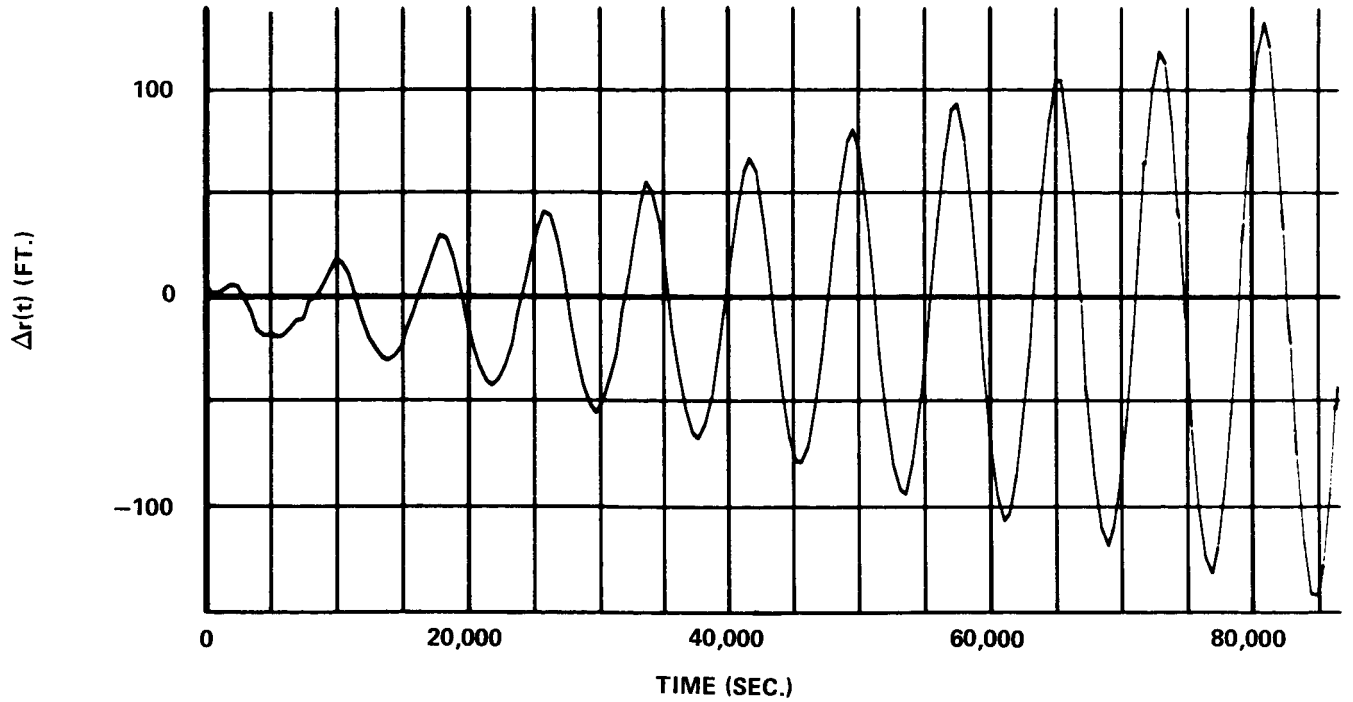

POSITION DIFFERENCE VS. TIME

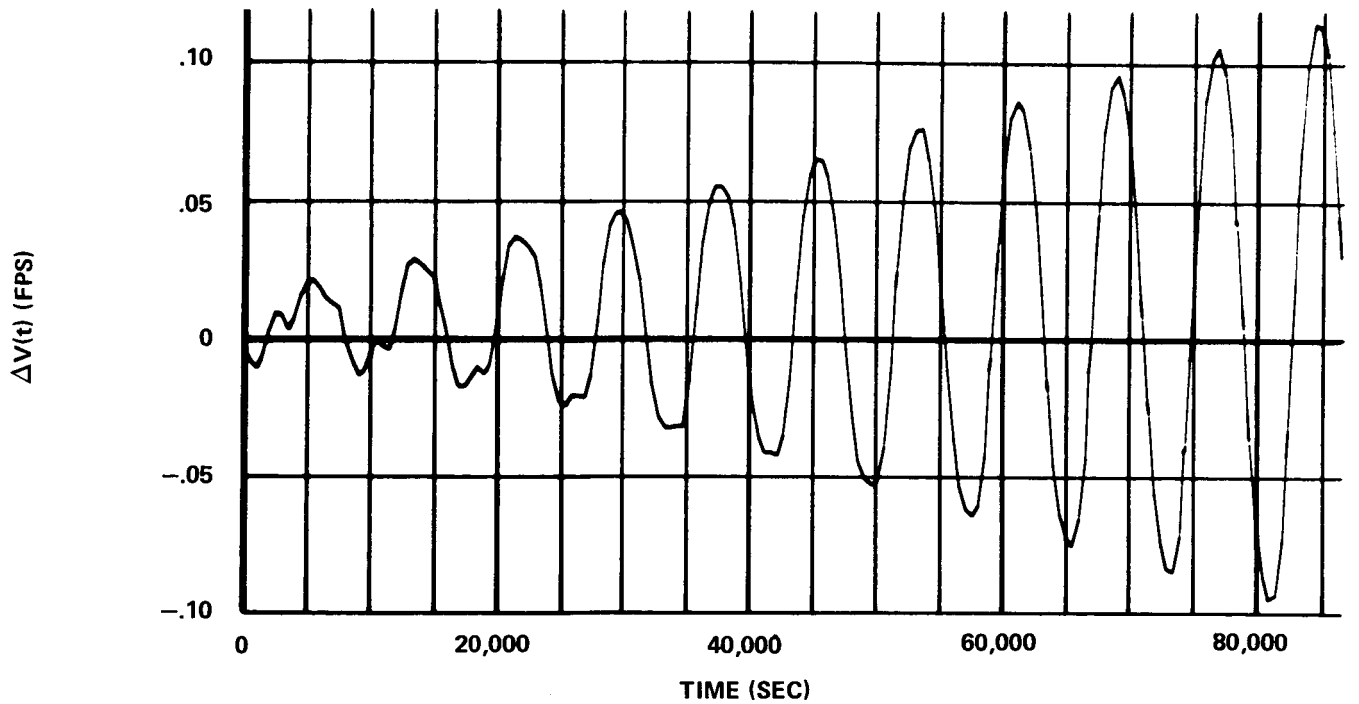

VELOCITY DIFFERENCE VS. TIME

FIGURE 22 - LUNAR ORBITER III ORBIT